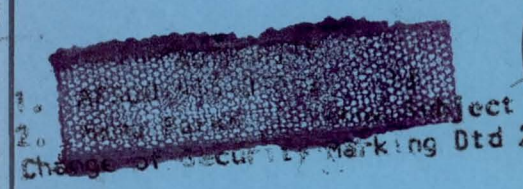
30
62 72247 Copy
609
UNCLASSIFIED CONFIDENTIAL
NASA TM X-423



Classification changed to declassifie
April
Authority of NASA CSM 2 by
Carroll.

N63-13904
code-1

TECHNICAL MEMORANDUM

X-423

STATIC LONGITUDINAL AERODYNAMIC CHARACTERISTICS AT TRANSONIC SPEEDS OF A LENTICULAR-SHAPED REENTRY VEHICLE

By John P. Mugler, Jr., and Walter B. Olstad

Langley Research Center
Langley Field, Va.



CLASSIFIED DOCUMENT - TITLE UNCLASSIFIED

This material contains information affecting the national defense of the United States within the meaning of the espionage laws, Title 18, U.S.C., Secs. 793 and 794, the transmission or revelation of which in any manner to an unauthorized person is prohibited by law.

NATIONAL AERONAUTICS AND SPACE ADMINISTRATION

WASHINGTON

December 1960

CONFIDENTIAL

UNCLASSIFIED
CONFIDENTIAL

NATIONAL AERONAUTICS AND SPACE ADMINISTRATION

TECHNICAL MEMORANDUM X-423

STATIC LONGITUDINAL AERODYNAMIC CHARACTERISTICS AT TRANSONIC SPEEDS OF A LENTICULAR-SHAPED REENTRY VEHICLE*

By John P. Mugler, Jr., and Walter B. Olstad

SUMMARY

Tests have been made at transonic speeds on a lenticular-shaped reentry vehicle. The tests covered a Mach number range from 0.40 to 1.20 at angles of attack from approximately -3° to 102°. Tests were made on body-alone and body-fin configurations. The Reynolds number based on body length varied during the tests from about 1.2×10^6 to 4.4×10^6.

The results indicate that the body-alone configuration was statically unstable at angles of attack near 0° and stable at angles of attack near 90°. Addition of horizontal fins with no deflection resulted in a neutrally stable configuration near 0° at most Mach numbers and slightly increased the stability at angles of attack near 90°. At transonic speeds and moderate angles of attack separated flow was prominent on the body upper surface and caused horizontal-fin ineffectiveness at these test conditions. Deflecting the fins -20° caused the configuration to trim at a higher angle of attack at all Mach numbers. Maximum lift-drag ratios of about 5.5 were obtained on both the body-alone and body-fin configurations at $M = 0.4$, and this value diminished to about 1.0 at low-supersonic speeds.

INTRODUCTION

At the present time the reentry requirements of space vehicles are not clearly defined, and vehicles having maximum lift-drag ratios from 0 to about 2 at hypersonic speeds are being studied. Therefore, an extensive investigation is in progress at the Langley Research Center to study the aerodynamic characteristics at subsonic to hypersonic speeds of a wide variety of generalized lifting-body shapes suitable for reentry vehicles. Since some of these vehicles may traverse a large

*Title, Unclassified.

portion of the flight path at high angles of attack, these studies generally cover a large angle range.

The present paper presents the static longitudinal aerodynamic characteristics at transonic speeds on one vehicle - a lenticular-shaped body with and without movable fins which provide longitudinal control. The tests on this lenticular-shaped vehicle were also made in support of studies currently being made by NASA Space Task Group. The tests were conducted in the Langley 8-foot transonic pressure tunnel at Mach numbers from 0.40 to 1.20 and at angles of attack up to approximately 100°. Tests on similar vehicles have been conducted at supersonic speeds and at low-subsonic speeds, and the results have been presented in references 1, 2, and 3.

SYMBOLS

C_A axial-force coefficient, $\frac{\text{Axial force}}{qS}$

C_D drag coefficient, $\frac{\text{Drag}}{qS}$

$C_{D,min}$ minimum drag coefficient

C_L lift coefficient, $\frac{\text{Lift}}{qS}$

C_m pitching-moment coefficient, $\frac{\text{Pitching moment about c.g.}}{qSl}$

(c.g. at $0.45l$, see fig. 1)

C_N normal-force coefficient, $\frac{\text{Normal force}}{qS}$

$C_{p,b}$ base-pressure coefficient, $\frac{p_b - p}{q}$

$(L/D)_{max}$ maximum lift-drag ratio

l	body length, in.
M	free-stream Mach number
p	free-stream static pressure, lb/sq ft
p_b	static pressure at model base, lb/sq ft
q	free-stream dynamic pressure, lb/sq ft
R	Reynolds number based on body length
S	body planform area, excluding fins, sq ft
α	angle of attack, deg
δ	fin deflection angle, positive when trailing edge down, deg

APPARATUS

Tunnel

The investigation was conducted in the Langley 8-foot transonic pressure tunnel. The test section of this facility is rectangular in cross section. The upper and lower walls are slotted longitudinally to allow continuous operation through the transonic speed range with negligible effects of choking and blockage. During this investigation the tunnel was operated at stagnation pressures from about 1/3 to 1 atmosphere. The dewpoint of the tunnel air was controlled and was kept constant at approximately 0° F. The stagnation temperature of the tunnel air was automatically controlled and was kept constant at about 120° F. Control of both dewpoint and stagnation temperature in this manner minimized humidity effects. Details of the test section are presented in reference 4.

Models

Details of the lenticular-shaped model used during this investigation are shown in figure 1, and photographs of the model are presented in figure 2. The body shape was generated by revolving an ellipse, having a major-to-minor-axis ratio of 2.73, about its minor axis. The horizontal fins were flat plates with the leading edges rounded and vertical end plates on the tips. The fin deflection angle δ is the angle generated by rotating the horizontal fin about its hinge line and is positive when the trailing edge of the fin is deflected down. The end plates were

rigidly attached to the horizontal fins so that the entire fin structure was deflected.

At angles of attack from about -3° to 20° the model was supported in the tunnel by a conventional sting which extended from the base of the body and was, in turn, attached to the central support system of the tunnel. (See figs. 1(a) and 2(a).) A three-component internal strain-gage balance was attached to the forward end of the sting and was housed within the body. At angles of attack greater than 20° an adapter was attached to the forward end of the sting and fitted into a cavity on top of the body. (See figs. 1(b) and 2(b).) The movable tongue of the adapter, which was attached to the balance, was fixed at angles from 20° to 90° to obtain data at the high angles of attack. When the adapter was used, a base plug was fitted into the hole at the model base provided for the low-angle sting. (See figs. 1(b) and 2(b).) These support systems kept the model near the center line of the tunnel at all angles of attack.

TESTS

Tests were made on the body alone, body-fin combination with no fin deflection ($\delta = 0°$), and on the body-fin combination with the fins deflected 20°, trailing edge up ($\delta = -20°$). The measured fin deflection angles are as follows:

Fin	Measured fin deflection angles, deg, for -	
	$\delta = 0°$	$\delta = -20°$
Right	-0.63	-21.60
Left	.03	-20.87

The nominal deflection angles of 0° and -20° will be used in the remainder of the paper.

Tests were made at Mach numbers from 0.40 to 1.20 at angles of attack from about -3° to 102°. At Mach numbers between 1.03 and 1.13, boundary reflected disturbances influenced the model so no data were recorded in this Mach number range.

Tests were made at stagnation pressures from about 1/3 to 1 atmosphere depending on Mach number and angle of attack. Therefore, the Reynolds number based on body length varied during the tests from about 1.2×10^6 to 4.4×10^6. (See fig. 3.) Trajectory calculations for a full-scale vehicle of this shape indicate that the flight Reynolds number based on body length for a typical reentry flight plan might vary from about 4.9×10^6 at $M = 1.2$ to 8.5×10^6 at $M = 0.6$.

All tests were made with natural transition.

MEASUREMENTS AND ACCURACY

A study of the factors affecting the accuracy of the results indicates that the measured coefficients are accurate within the following limits:

M	Accuracy of -		
	C_N	C_A	C_m
0.40	±0.054	±0.0038	±0.0090
.60	±.028	±.0019	±.0046
1.20	±.028	±.0019	±.0045

The angle of attack which was measured with a strain-gage attitude transmitter mounted in the tunnel central support tube was adjusted for flow angularity and balance and sting deflections under load. The angle of attack is estimated to be accurate within $\pm 0.1^\circ$.

Calibrations of the tunnel test section indicate that local deviations from the average free-stream Mach number are of the order of ±0.005 at subsonic speeds. With increases in Mach number, these deviations increase but do not exceed ±0.010 in the region of the model at $M = 1.20$. Several representative Mach number distributions along the center of the test section are presented in reference 4. The average free-stream Mach number was held to within ±0.005 of the nominal values shown in this paper.

The pressure in the region of the model base was measured during the tests and is presented as base-pressure coefficient in figure 4. For the low-angle tests (α = -3° to 20°) the base-pressure tube was mounted on the sting several inches forward of the model base. For the high-angle tests (α = 20° to 102°) the base-pressure tube was located near the bottom of the cavity provided for the knuckle. It is estimated that the accuracy of these base-pressure coefficients is within ±0.010.

CORRECTIONS

No corrections have been applied to the data for boundary-interference effects. At subsonic speeds, the slotted test section minimized boundary-interference effects such as blockage and boundary-induced upwash.

The effects of the presence of the high-angle knuckle were not determined during these tests, and no corrections have been applied to the data to account for support interference. The axial and drag data presented have not been adjusted to free-stream conditions at the model base.

RESULTS

The aerodynamic coefficients plotted against angle of attack for the three configurations tested are presented in figure 5. These coefficients are also tabulated in tables I, II, and III along with the base-pressure coefficients. At a Mach number of 0.80 no data were obtained at angles of attack below about 20° for the body-alone configuration. For the body-fin, δ = -20° configuration the highest test angle of attack was about 73°. As was noted previously, the high-angle adapter was installed near 20° to obtain data at high angles of attack. Data at angles of attack of approximately 20° were also obtained using the low-angle sting. (See tables I to III.) In most cases the data obtained using both support systems agreed reasonably well; however, in some instances the agreement was poor. Therefore, the fairings of the curves in figure 5 in the region of 20° are rather arbitrary. Figure 6 presents schlieren photographs taken during the tests of the body-alone configuration at an angle of attack of approximately 20°. Figures 7, 8, 9, and 10 present analysis curves. The slopes in figure 7 were taken at angles of attack between -3° and 4°. The slopes in figure 9 were taken at angles of attack between 82° and 102°. The other quantities in figures 7 to 10 were obtained from the faired curves.

DISCUSSION

Body-Alone Configuration

The aerodynamic characteristics for the body-alone configuration shown in figure 5 show that the lift curve has a positive slope up to an angle of attack of about 30° or 40° (maximum lift) and a negative slope over the remainder of the angle range tested. As would be expected, the drag coefficients reach a maximum around an angle of attack of 90°. The pitching-moment-coefficient curves (c.g. at 45 percent of the body length) have a positive slope up to about the angle of attack for maximum lift and then a negative slope over the remainder of the angle range. The normal-force coefficients appear to be reaching a maximum value at angles of attack near 100°. At Mach numbers of 0.80 and above, the axial-force coefficients generally decrease with increasing angle of attack from a positive value at -3° to 0 at an angle of attack of approximately 90°. At a Mach number of 0.60, negative values of the axial-force coefficient were obtained at angles of attack near 30°, probably because of leading-edge thrust developed by this configuration.

The schlieren photographs at $\alpha \approx 20°$ for the body-alone configuration presented in figure 6 show that at Mach numbers of 0.80 and 0.95 a large separated wedge is formed on the body upper surface. With increases in Mach number this separated region diminishes in thickness and extent. At Mach numbers of 1.13 and 1.20 the strong shock indicated by the broad white line is the model bow wave striking the tunnel wall.

The lift-curve slope at angles of attack near 0° (fig. 7(a)) for the body-alone configuration was about 0.01 at the low Mach numbers and increased at transonic speeds to a value of about 0.022. The moment characteristics at angles of attack near 0° (fig. 7(b)) indicate that the body-alone configuration is statically unstable throughout the entire Mach number range tested. The minimum-drag curve (fig. 7(c)) exhibits typical drag-rise characteristics at transonic speeds. The maximum lift-drag-ratio characteristics (fig. 8) show that a maximum lift-drag ratio of about 5.5 was obtained at $M = 0.4$. With increases in Mach number, the maximum lift-drag ratio decreased rapidly to about $M = 0.90$ where it leveled out at a value of about 1.0. The lift coefficient for maximum lift-drag ratio increased with increases in Mach number from about 0.04 at $M = 0.4$ to about 0.44 at $M = 1.2$. The angle of attack for maximum lift-drag ratio increased with increases in Mach number from about 4° at $M = 0.4$ to 20° at $M = 1.2$.

At angles of attack near 90° the lift-curve slope for the body-alone configuration has a negative value of about -0.011 at Mach numbers from 0.6 to 0.8 (fig. 9(a)). Further increases in Mach number cause the lift-curve slope to increase negatively to a value of about -0.016 at a Mach

number of 1.2. The slope of the pitching-moment curves at angles of attack near 90° for the body-alone configuration (fig. 9(b)) is constant through the Mach number range tested and indicates that the body alone is statically stable. The drag coefficient at an angle of attack of 90° gradually increases with increases in Mach number up to a Mach number of about 1.1 and did not exhibit the pronounced drag-rise characteristics noted at an angle of attack of 0°.

In reference 5 it was pointed out that for flat wings a good approximation of the lift-curve slope (per radian) at an angle of attack of 90° was the negative of the drag coefficient at an angle of attack of 90°; therefore,

$$\left(\frac{\partial C_L}{\partial \alpha}\right)_{\alpha=90^\circ} \approx -C_{D,\alpha=90^\circ} \tag{1}$$

The basis for this approximation can be seen by noting that

$$C_L = C_N \cos \alpha - C_A \sin \alpha \tag{2}$$

then

$$\frac{\partial C_L}{\partial \alpha} = -\left(C_N + \frac{\partial C_A}{\partial \alpha}\right) \sin \alpha + \left(\frac{\partial C_N}{\partial \alpha} - C_A\right) \cos \alpha \tag{3}$$

and at an angle of attack of 90°

$$\left(\frac{\partial C_L}{\partial \alpha}\right)_{\alpha=90^\circ} = -C_{N,\alpha=90^\circ} - \left(\frac{\partial C_A}{\partial \alpha}\right)_{\alpha=90^\circ} \tag{4}$$

but

$$C_D = C_A \cos \alpha + C_N \sin \alpha \tag{5}$$

and at an angle of attack of 90°

$$C_{D,\alpha=90^\circ} = \left(C_N\right)_{\alpha=90^\circ} \tag{6}$$

therefore

$$\left(\frac{\partial C_L}{\partial \alpha}\right)_{\alpha=90^\circ} = -C_{D,\alpha=90^\circ} - \left(\frac{\partial C_A}{\partial \alpha}\right)_{\alpha=90^\circ} \quad (7)$$

It was noted in reference 5 that the value of $\left(\frac{\partial C_A}{\partial \alpha}\right)$ was small for flat wings, generally less than 2 percent of the value of the drag coefficient at 90°, and can therefore be neglected to give equation (1). It is of interest to note that for the present configuration this approximation is not valid. Figures 9(c) and (d) show that the contribution of $\left(\frac{\partial C_A}{\partial \alpha}\right)_{\alpha\approx 90^\circ}$ is of the order of 25 percent of $C_{D,\alpha=90^\circ}$ and neglecting it would result in values of $\left(\frac{\partial C_L}{\partial \alpha}\right)_{\alpha\approx 90^\circ}$ which were of the order of 30 percent too high.

Body-Fin, $\delta = 0^\circ$ Configuration

The effects on the basic aerodynamic characteristics of adding the horizontal fin to the body-alone configuration can be seen in figure 5. The addition of the fin generally caused the angle of attack at which maximum lift occurred to increase, caused the drag coefficient to increase at all test conditions, and caused marked changes in the pitching-moment characteristics. An interesting effect is evident at Mach numbers of 0.90 and 0.95 at angles of attack from about -3° to 20°. At these test conditions the addition of the horizontal fin caused little or no change in the lift- and pitching-moment-coefficient characteristics. The schlieren photographs previously noted for the body-alone configuration (fig. 6) indicate that a large portion of the horizontal fins may have been blanketed by the separated upper-surface flow and thus were ineffective. The schlieren photographs indicate that this condition is gradually diminished with increases in Mach number and the lift- and pitching-moment-coefficient data in figures 5(a) and (c), respectively, are consistent with this premise.

At low angles of attack the addition of the horizontal fin caused large increases in the lift-curve slope up to a Mach number of about 0.8 and some increases above $M = 1.0$ (fig. 7(a)). Even though the addition of the fin decreased the slope of the pitching-moment-coefficient curve at all Mach numbers at $\alpha \approx 0^\circ$, the body-fin, $\delta = 0^\circ$ configuration was still unstable or neutrally stable at all Mach numbers below about 1.0 (fig. 7(b)). The minimum drag coefficient for the body-fin, $\delta = 0^\circ$ configuration was generally increased slightly over the body-alone values (fig. 7(c)).

The maximum lift-drag-ratio characteristics (fig. 8) indicate that the addition of the fin produced little or no change in the maximum lift-drag ratio. The addition of the fin was responsible for some increases in the lift coefficient and angle of attack for maximum lift-drag ratio.

At angles of attack near 90° the addition of the fin caused an increase in the negative lift-curve slope, a slight increase in the negative pitching-moment-curve slope, and a rather large increase in the drag coefficient (fig. 9).

Body-Fin, $\delta = -20^\circ$ Configuration

The effects of deflecting the fin -20° (trailing edge up) on the basic aerodynamic characteristics can be seen in figure 5. The ineffectiveness of the fins to produce lift and pitch increments at Mach numbers of 0.90 and 0.95 at moderate angles of attack is evident for the $\delta = -20^\circ$ fin configuration as it was for the $\delta = 0^\circ$ configuration. (See figs. 5(a) and (c).) However, the angle-of-attack range over which this ineffectiveness occurred was reduced to about $7\frac{1}{2}^\circ$ to 20° for the $\delta = -20^\circ$ fin configuration as compared to about -3° to 20° for the $\delta = 0^\circ$ fin configuration. As would be expected, the body-fin, $\delta = -20^\circ$ configuration trimmed at a higher angle of attack at all Mach numbers than the $\delta = 0^\circ$ configuration (fig. 5(c)). It is likely that the model could be trimmed at intermediate angles of attack by using suitable fin deflections between 0° and -20°. The incremental pitching-moment coefficients due to a fin deflection of -20° are plotted against the angle of attack in figure 10. At Mach numbers above 0.60, these incremental pitching-moment coefficients exhibited a minimum value at angles of attack around 15° to 25° and at Mach numbers of 0.90 and 0.95, the value dropped to about 0 at an angle of attack of approximately 15°. This reduction in the pitching-moment-coefficient increment is a result of the separated flow prevalent on the body upper surface that was noted previously.

CONCLUSIONS

Analysis of data from tests at transonic speeds on a lenticular-shaped reentry vehicle has led to the following conclusions:

1. The body-alone configuration was statically unstable at angles of attack near 0° but was stable at angles of attack near 90°. Maximum lift-drag ratios of about 5.5 were obtained for the body-alone configuration at a Mach number of 0.4 but diminished to about 1.0 at low-supersonic speeds.

2. The addition of horizontal fins with no deflection decreased the slope of the pitching-moment-coefficient curves at angles of attack near 0°, but this configuration was still neutrally stable or unstable over most of the Mach number range. At angles of attack near 90° the addition of the fins resulted in slightly increased stability over the Mach number range. The addition of fins had little or no effect on the maximum lift-drag ratio.

3. At transonic speeds and moderate angles of attack, separated flow was prevalent on the body upper surface. As a result of this, the fins were not effective at these test conditions.

4. Deflecting the fins -20° caused the configuration to trim at a higher angle of attack at all Mach numbers.

Langley Research Center,
National Aeronautics and Space Administration,
Langley Field, Va., September 1, 1960.

REFERENCES

1. Jackson, Charlie M., Jr., and Harris, Roy V., Jr.: Static Longitudinal Stability and Control Characteristics at a Mach Number of 1.99 of a Lenticular-Shaped Reentry Vehicle. NASA TN D-514, 1960.

2. Letko, William: Experimental Investigation at a Mach Number of 3.11 of the Lift, Drag, and Pitching-Moment Characteristics of Five Blunt Lifting Bodies. NASA TN D-226, 1960.

3. Ware, George M.: Static Stability and Control Characteristics at Low-Subsonic Speeds of a Lenticular Reentry Configuration. NASA TM X-431, 1960.

4. Mugler, John P., Jr.: Transonic Wind-Tunnel Investigation of the Aerodynamic Loading Characteristics of a 60° Delta Wing in the Presence of a Body With and Without Indentation. NACA RM L55G11, 1955.

5. Phillips, William H.: Research on Blunt-Faced Entry Configurations at Angles of Attack Between 60° and 90°. NASA TM X-315, 1960.

CONFIDENTIAL

TABLE I.- AERODYNAMIC COEFFICIENTS FOR BODY-ALONE CONFIGURATION

	α, deg	C_L	C_D	C_m	C_N	C_A	$C_{p,b}$
				M = 0.40			
Low-angle sting	-3.0	-0.022	0.0039	-0.0300	-0.022	0.0027	0.3339
	.0	.019	.0040	-.0051	.019	.0040	.3626
	.0	.019	.0040	-.0037	.019	.0040	.3628
	.0	.000	.0009	.0010	.000	.0009	.0000
	4.0	.042	.0057	.0382	.042	.0027	.3555
	8.1	.082	.0144	.0733	.083	.0027	.3125
	12.1	.140	.0277	.1047	.143	-.0024	.2550
	16.2	.196	.0501	.1302	.202	-.0064	.1904
	20.2	.279	.0780	.1501	.289	-.0230	.1688
				M = 0.60			
Low-angle sting	-3.0	-0.008	0.0152	-0.0333	-0.009	0.0147	0.2749
	.0	.028	.0150	-.0064	.028	.0150	.2908
	.0	.051	.0157	-.0104	.051	.0157	.2934
	4.1	.070	.0161	.0338	.071	.0111	.3027
	8.2	.120	.0271	.0704	.122	.0098	.2480
	12.2	.155	.0389	.1077	.159	.0052	.1804
	16.3	.218	.0548	.1386	.225	-.0086	.1713
	20.4	.298	.0827	.1615	.308	-.0265	.1605
High-angle adapter	20.5	.222	.0780	.1593	.235	-.0047	.1351
	20.5	.228	.0802	.1589	.242	-.0049	.1354
	31.0	.556	.2080	.1907	.583	-.1078	.0950
	41.0	.465	.4709	.1228	.660	.0506	-.4117
	50.9	.331	.5344	.0927	.623	.0802	-.4180
	50.9	.334	.5395	.0925	.629	.0809	-.4179
	60.9	.229	.6280	.0649	.660	.1049	-.3878
	70.9	.140	.7054	.0320	.713	.0980	-.3780
	80.9	.080	.7641	-.0069	.767	.0415	-.3625
	80.9	.072	.7655	-.0059	.767	.0493	-.3697
	90.9	-.020	.8161	-.0421	.816	.0072	-.3806
	100.9	-.137	.8303	-.0763	.841	-.0230	-.4362
				M = 0.80			
Low-angle sting	No low-angle data obtained						
High-angle adapter	21.1	0.386	0.2163	0.1216	0.437	0.0633	-0.1924
	21.1	.396	.2269	.1182	.451	.0691	-.2469
	21.1	.389	.2183	.1227	.442	.0637	-.1865
	31.3	.438	.4104	.1130	.588	.1229	-.4353
	41.4	.381	.5447	.0921	.646	.1573	-.4724
	51.5	.360	.6707	.0710	.749	.1352	-.4688
	51.5	.360	.6687	.0711	.747	.1347	-.4655
	61.6	.280	.7592	.0484	.801	.1150	-.4070
	71.6	.173	.8188	.0207	.831	.0952	-.3696
	81.5	.067	.8630	-.0106	.863	.0610	-.3510
	81.5	.066	.8588	-.0107	.859	.0610	-.3501
	91.5	-.039	.9123	-.0482	.913	.0141	-.3859
	101.5	-.140	.9148	-.0832	.924	-.0455	-.4135
				M = 0.90			
Low-angle sting	-3.1	-0.088	0.1729	-0.0118	-0.097	0.1679	-0.2359
	.0	-.039	.1727	.0059	-.039	.1727	-.2409
	4.1	.062	.1796	.0241	.075	.1747	-.2423
	8.1	.136	.1895	.0442	.161	.1694	-.2316
	12.2	.227	.2229	.0580	.269	.1698	-.2702
	16.3	.262	.2629	.0677	.325	.1790	-.2908
	20.3	.283	.3141	.0707	.375	.1962	-.3435
High-angle adapter	20.9	.353	.3181	.0916	.443	.1717	-.3991
	20.9	.355	.3202	.0927	.446	.1728	-.3934
	31.1	.388	.4623	.0901	.571	.1959	-.4768
	41.2	.409	.6081	.0737	.708	.1876	-.4952
	51.6	.394	.7510	.0606	.833	.1574	-.4859
	51.6	.391	.7454	.0602	.827	.1565	-.4793
	61.7	.323	.8609	.0371	.911	.1236	-.4356
	71.7	.212	.9205	.0103	.940	.0878	-.3848
	81.9	.083	.9525	-.0170	.955	.0515	-.3533
	81.9	.084	.9542	-.0171	.957	.0503	-.3541
	91.9	-.042	.9929	-.0528	.994	.0090	-.3782
	101.9	-.167	1.0037	-.0857	1.017	-.0429	-.4224
				M = 0.95			
Low-angle sting	-3.1	-0.092	0.2186	-0.0125	-0.103	0.2133	-0.3329
	-3.1	-.083	.1640	-.0112	-.092	.1593	-.2237
	.0	-.032	.1624	.0054	-.032	.1624	-.2295
	.0	-.017	.2118	.0016	-.017	.2118	-.3191
	.0	-.022	.2122	.0009	-.022	.2122	-.3164
	4.1	.067	.2133	.0226	.082	.2080	-.3152
	8.2	.144	.2260	.0419	.174	.2033	-.2976
	12.3	.241	.2677	.0553	.293	.2103	-.3610
	16.3	.284	.3034	.0643	.358	.2114	-.3755
	20.4	.361	.3775	.0720	.470	.2279	-.4487
High-angle adapter	20.8	.375	.3713	.0845	.483	.2137	-.4651
	20.8	.384	.3732	.0838	.491	.2125	-.4653
	31.0	.407	.4940	.0751	.603	.2145	-.5259
	41.2	.445	.6439	.0665	.759	.1919	-.5045
	51.6	.441	.8312	.0542	.925	.1703	-.5344
	51.7	.449	.8432	.0536	.940	.1712	-.5438
	61.7	.357	.9339	.0313	.992	.1285	-.4618
	71.7	.235	.9941	.0040	1.017	.0899	-.4080
	81.9	.095	1.0062	-.0213	1.010	.0479	-.3622
	81.9	.096	1.0096	-.0209	1.013	.0476	-.3665
	91.9	-.045	1.0565	-.0579	1.057	.0102	-.4039
	101.9	-.178	1.0587	-.0878	1.073	-.0439	-.4291

	α, deg	C_L	C_D	C_m	C_N	C_A	$C_{p,b}$
				M = 1.00			
Low-angle sting	-3.1	-0.090	0.2579	-0.0123	-0.103	0.2527	-0.3445
	.0	-.016	.2488	.0015	-.016	.2488	-.3307
	.0	-.016	.2500	.0015	-.016	.2500	-.3308
	4.1	.075	.2530	.0184	.093	.2470	-.3411
	8.2	.179	.2803	.0356	.217	.2520	-.3728
	12.3	.274	.3205	.0505	.336	.2547	-.4080
	16.4	.347	.3582	.0631	.434	.2457	-.4376
	20.5	.395	.4049	.0702	.512	.2414	-.4649
High-angle adapter	20.8	.435	.4411	.0791	.564	.2579	-.5088
	20.8	.446	.4455	.0790	.575	.2581	-.5119
	31.0	.507	.5894	.0740	.738	.2444	-.6422
	41.1	.521	.7304	.0640	.873	.2075	-.5835
	51.6	.473	.8733	.0486	.978	.1727	-.5442
	51.6	.470	.8692	.0490	.973	.1722	-.5438
	61.6	.386	.9937	.0263	1.058	.1324	-.4938
	71.7	.266	1.0742	.0005	1.103	.0860	-.4505
	81.9	.107	1.0681	-.0242	1.073	.0449	-.3920
	81.9	.107	1.0774	-.0250	1.082	.0458	-.3981
	91.9	-.045	1.1028	-.0595	1.104	.0089	-.4124
	101.8	-.190	1.1131	-.0900	1.128	-.0423	-.4523
				M = 1.03			
Low-angle sting	-3.1	-0.087	0.2701	-0.0120	-0.101	0.2651	-0.3386
	.0	-.020	.2628	.0017	-.020	.2628	-.3269
	.0	-.015	.2632	.0023	-.015	.2632	-.3257
	4.1	.077	.2692	.0186	.096	.2631	-.3524
	8.2	.181	.2962	.0343	.222	.2673	-.3962
	12.3	.282	.3383	.0485	.348	.2703	-.4292
	16.4	.370	.3850	.0592	.464	.2647	-.4578
	20.5	.436	.4437	.0689	.564	.2627	-.5494
High-angle adapter	20.8	.438	.4449	.0751	.567	.2607	-.4830
	20.8	.446	.4477	.0757	.576	.2603	-.4861
	31.0	.507	.5871	.0726	.737	.2427	-.6160
	41.1	.519	.7276	.0623	.869	.2074	-.5672
	51.6	.490	.8995	.0456	1.009	.1742	-.5467
	51.6	.486	.8942	.0468	1.003	.1737	-.5450
	61.7	.400	1.0235	.0242	1.091	.1327	-.4950
	71.7	.273	1.1026	-.0017	1.133	.0864	-.4575
	82.0	.112	1.1090	-.0260	1.114	.0435	-.4071
	82.0	.110	1.1034	-.0263	1.108	.0416	-.4073
	92.0	-.050	1.1424	-.0626	1.144	.0102	-.4324
	102.0	-.201	1.1556	-.0922	1.172	-.0428	-.4651
				M = 1.13			
Low-angle sting	-3.1	-0.082	0.2559	-0.0114	-0.095	0.2512	-0.2149
	.0	-.021	.2473	.0018	-.021	.2473	-.2017
	.0	-.021	.2469	.0009	-.021	.2469	-.2036
	4.1	.067	.2495	.0176	.085	.2441	-.2303
	8.2	.157	.2754	.0324	.194	.2502	-.2637
	12.3	.258	.3192	.0448	.320	.2571	-.3011
	16.4	.338	.3662	.0554	.428	.2560	-.3298
	20.5	.425	.4360	.0628	.551	.2597	-.4118
High-angle adapter	20.8	.404	.4182	.0713	.526	.2479	-.3674
	20.8	.413	.4223	.0705	.536	.2485	-.3697
	31.0	.501	.5748	.0680	.725	.2349	-.4789
	41.2	.528	.7346	.0586	.881	.2055	-.4623
	51.5	.483	.8763	.0424	.987	.1681	-.4325
	51.5	.484	.8774	.0428	.988	.1681	-.4328
	61.5	.393	.9875	.0211	1.055	.1259	-.3705
	71.6	.277	1.0935	-.0035	1.125	.0833	-.3534
	82.1	.106	1.1036	-.0291	1.108	.0459	-.3178
	82.1	.108	1.1065	-.0288	1.111	.0446	-.3169
	92.1	-.052	1.1475	-.0632	1.149	.0099	-.3497
	102.1	-.203	1.1615	-.0902	1.178	-.0452	-.3777
				M = 1.20			
Low-angle sting	-3.1	-0.066	0.2981	-0.0123	-0.082	0.2941	-0.3053
	.0	-.011	.2914	.0013	-.011	.2914	-.2829
	.0	-.020	.2890	.0017	-.020	.2890	-.2876
	4.1	.080	.2994	.0169	.101	.2929	-.3464
	8.2	.168	.3228	.0317	.212	.2955	-.3675
	12.3	.266	.3641	.0427	.337	.2992	-.3948
	16.4	.360	.4168	.0506	.463	.2982	-.4170
	20.5	.460	.4917	.0562	.603	.2995	-.4638
High-angle adapter	20.7	.432	.4669	.0610	.569	.2840	-.3381
	20.7	.441	.4716	.0611	.579	.2851	-.3394
	30.9	.542	.6257	.0643	.786	.2581	-.5229
	41.0	.510	.7140	.0581	.853	.2045	-.4049
	51.5	.466	.8506	.0423	.956	.1657	-.3535
	51.5	.466	.8497	.0427	.955	.1650	-.3503
	61.5	.378	.9538	.0215	1.019	.1229	-.2818
	71.6	.267	1.0600	-.0029	1.090	.0824	-.2636
	82.1	.104	1.0765	-.0282	1.081	.0440	-.2315
	92.1	-.052	1.1227	-.0605	1.124	.0101	-.2635
	102.2	-.205	1.1470	-.0877	1.164	-.0412	-.3061

CONFIDENTIAL

UNCLASSIFIED

TABLE II.- AERODYNAMIC COEFFICIENTS FOR THE BODY-FIN CONFIGURATION

[$\delta = 0^\circ$]

	α, deg	C_L	C_D	C_m	C_N	C_A	$C_{p,b}$
				M = 0.40			
Low-angle sting	-3.1	-0.354	0.0801	0.0598	-0.358	0.0607	0.2264
	-3.1	-.233	.0805	.0575	-.237	.0679	.2588
	-.1	-.236	.0522	.0575	-.237	.0519	.2552
	4.0	-.052	.0270	.0538	-.050	.0306	.2733
	8.1	.125	.0240	.0505	.128	.0062	.3093
	12.1	.282	.0514	.0451	.286	-.0090	.2663
	16.2	.472	.0993	.0248	.481	-.0363	.3131
	20.3	.614	.1565	.0169	.630	-.0658	.2918
				M = 0.60			
Low-angle sting	-3.2	-0.323	0.0850	0.0509	-0.327	0.0667	0.1626
	-.1	-.189	.0570	.0507	-.189	.0567	.1930
	-.1	-.193	.0570	.0500	-.193	.0566	.1944
	4.0	-.034	.0321	.0562	-.032	.0344	.2578
	8.2	.141	.0290	.0529	.144	.0087	.2752
	12.3	.262	.0558	.0588	.268	-.0012	.2809
	16.4	.446	.1010	.0416	.456	-.0292	.2882
	20.5	.601	.1568	.0368	.617	-.0639	.2828
High-angle adapter	20.7	.514	.1560	.0399	.536	-.0357	.0938
	20.7	.511	.1541	.0385	.532	-.0364	.0962
	31.2	.870	.3579	.0265	.929	-.1437	.0195
	41.2	.773	.6453	-.0319	1.007	-.0233	-.4228
	51.2	.734	.8348	-.0924	1.110	-.0485	-.5224
	51.2	.726	.8324	-.0941	1.104	-.0444	-.5199
	61.3	.649	1.0572	-.1436	1.259	-.0611	-.5199
	71.3	.537	1.2298	-.1904	1.337	-.1152	-.4883
	81.2	.339	1.3595	-.2270	1.395	-.1271	-.4582
	81.2	.338	1.3610	-.2272	1.397	-.1263	-.4586
	91.2	.149	1.4085	-.2665	1.405	-.1778	-.4204
	101.1	-.030	1.4000	-.3081	1.380	-.2393	-.4165
				M = 0.80			
Low-angle sting	-3.2	-0.315	0.0925	0.0501	-0.320	0.0750	0.1740
	-.1	-.166	.0661	.0494	-.167	.0659	.1641
	-.1	-.179	.0649	.0499	-.179	.0647	.1712
	4.1	.052	.0573	.0428	.056	.0534	.1421
	8.2	.213	.0832	.0476	.223	.0521	.1593
	12.3	.338	.1242	.0508	.357	.0496	.1127
	16.3	.431	.1829	.0522	.465	.0544	.0588
	20.4	.510	.2703	.0425	.572	.0758	.0441
High-angle adapter	21.2	.539	.2538	.0469	.594	.0422	-.1866
	31.4	.601	.4826	.0108	.765	.0987	-.4313
	41.7	.685	.7316	-.0505	.998	.0911	-.5295
	51.9	.698	.9340	-.1034	1.166	.0273	-.5140
	51.9	.693	.9333	-.1034	1.163	.0297	-.5129
	62.1	.655	1.1776	-.1540	1.347	-.0274	-.4999
	72.2	.537	1.3680	-.2008	1.467	-.0926	-.4837
	81.4	.354	1.4907	-.2469	1.527	-.1280	-.4768
	81.5	.352	1.4926	-.2477	1.528	-.1276	-.4778
	91.5	.144	1.5640	-.2914	1.560	-.1843	-.4721
	101.3	-.065	1.5702	-.3325	1.553	-.2445	-.4756
				M = 0.90			
Low-angle sting	-3.1	-0.109	0.1765	0.0046	-0.118	0.1704	-0.2258
	.0	-.018	.1723	.0055	-.018	.1723	-.2344
	.0	-.017	.1732	.0072	-.017	.1732	-.2362
	4.1	.089	.1821	.0157	.102	.1752	-.2301
	8.2	.157	.1932	.0327	.183	.1690	-.2152
	12.2	.221	.2235	.0461	.263	.1717	-.2345
	16.3	.255	.2619	.0522	.318	.1800	-.2910
	20.3	.268	.3069	.0540	.357	.1951	-.3554
High-angle adapter	20.9	.384	.3340	.0558	.478	.1749	-.3949
	20.9	.353	.3256	.0592	.445	.1786	-.3896
	31.2	.502	.5295	.0054	.703	.1931	-.5037
	41.6	.676	.7820	-.0577	1.025	.1361	-.5371
	52.3	.716	1.0185	-.1094	1.244	.0570	-.5300
	52.3	.717	1.0198	-.1101	1.246	.0566	-.5309
	62.6	.688	1.2881	-.1706	1.460	-.0170	-.5256
	72.7	.551	1.4746	-.2180	1.572	-.0871	-.4972
	81.3	.388	1.5895	-.2600	1.630	-.1440	-.4886
	81.3	.383	1.5945	-.2605	1.634	-.1386	-.4892
	91.3	.159	1.6673	-.3051	1.663	-.1977	-.4605
	101.3	-.079	1.7010	-.3482	1.684	-.2559	-.5045
				M = 0.95			
Low-angle sting	-3.1	-0.096	0.2211	-0.0035	-0.108	0.2156	-0.2896
	.0	-.022	.2147	.0063	-.022	.2147	-.2937
	.0	-.016	.2148	.0052	-.016	.2148	-.2910
	4.1	.077	.2162	.0168	.092	.2102	-.2794
	8.2	.163	.2343	.0302	.195	.2088	-.2694
	12.3	.245	.2662	.0406	.296	.2082	-.2965
	16.3	.292	.3052	.0501	.366	.2110	-.3638
	20.4	.337	.3537	.0461	.439	.2143	-.3902
High-angle adapter	20.9	.456	.3966	.0427	.568	.2075	-.4568
	20.9	.460	.3975	.0428	.572	.2070	-.4567
	31.1	.541	.5726	-.0032	.759	.2109	-.5294
	41.5	.738	.8404	-.0714	1.110	.1403	-.5624
	52.6	.760	1.0932	-.1226	1.330	.0609	-.5599
	52.6	.762	1.0944	-.1224	1.332	.0606	-.5613
	62.8	.715	1.3552	-.1833	1.532	-.0172	-.5389
	73.0	.570	1.5471	-.2297	1.646	-.0917	-.5090
	81.5	.396	1.6316	-.2659	1.672	-.1485	-.4794
	81.5	.395	1.6300	-.2656	1.671	-.1484	-.4789
	91.4	.157	1.7156	-.3110	1.711	-.1998	-.4753
	101.4	-.081	1.7194	-.3485	1.702	-.2598	-.4749

	α, deg	C_L	C_D	C_m	C_N	C_A	$C_{p,b}$
				M = 1.00			
Low-angle sting	-3.1	-0.159	0.2872	0.0282	-0.174	0.2782	-0.4007
	.0	-.039	.2674	.0175	-.039	.2674	-.3710
	.0	-.038	.2671	.0174	-.039	.2671	-.3700
	4.1	.089	.2692	.0167	.108	.2622	-.3501
	8.2	.225	.2899	.0124	.265	.2547	-.3774
	12.3	.343	.3338	.0174	.407	.2527	-.4179
	16.4	.427	.3836	.0260	.518	.2474	-.4300
	20.5	.506	.4391	.0196	.627	.2342	-.3716
High-angle adapter	20.9	.562	.4692	.0156	.692	.2377	-.4797
	20.9	.565	.4706	.0160	.696	.2378	-.4815
	31.1	.667	.6596	-.0216	.912	.2195	-.5968
	41.4	.811	.9050	-.0871	1.207	.1427	-.6031
	52.3	.815	1.1604	-.1339	1.416	.0657	-.5861
	52.3	.815	1.1595	-.1340	1.416	.0650	-.5848
	62.5	.755	1.4203	-.1909	1.609	-.0138	-.5437
	72.6	.599	1.6008	-.2409	1.707	-.0909	-.5245
	81.5	.411	1.6995	-.2775	1.742	-.1548	-.4852
	81.5	.412	1.7001	-.2779	1.742	-.1556	-.4849
	91.5	.163	1.7588	-.3169	1.754	-.2076	-.4634
	101.4	-.081	1.7522	-.3520	1.734	-.2650	-.4730
				M = 1.03			
Low-angle sting	-3.1	-0.177	0.3049	0.0363	-0.194	0.2948	-0.4157
	.0	-.052	.2857	.0231	-.052	.2857	-.3870
	.0	-.052	.2859	.0231	-.052	.2859	-.3867
	4.1	.090	.2856	.0153	.111	.2784	-.3707
	8.2	.246	.3092	.0062	.288	.2707	-.4000
	12.4	.371	.3529	.0067	.437	.2654	-.4232
	16.4	.460	.4071	.0140	.557	.2601	-.4153
	20.5	.563	.4729	.0041	.693	.2455	-.3172
High-angle adapter	20.9	.576	.4793	.0095	.709	.2424	-.4433
	20.9	.578	.4805	.0086	.712	.2425	-.4464
	31.2	.709	.6809	-.0276	.959	.2156	-.5855
	41.4	.840	.9326	-.0937	1.247	.1433	-.6069
	52.4	.827	1.1757	-.1372	1.436	.0633	-.5740
	52.4	.828	1.1760	-.1378	1.437	.0621	-.5721
	62.6	.765	1.4363	-.1935	1.627	-.0172	-.5294
	72.7	.607	1.6258	-.2457	1.733	-.0950	-.5059
	81.4	.418	1.7188	-.2813	1.762	-.1562	-.4859
	81.4	.419	1.7241	-.2818	1.767	-.1562	-.4864
	91.4	.167	1.7627	-.3173	1.758	-.2089	-.4606
	101.3	-.082	1.7819	-.3564	1.763	-.2688	-.4741
				M = 1.13			
Low-angle sting	-3.1	-0.168	0.2884	0.0332	-0.183	0.2789	-0.2857
	.0	-.049	.2693	.0214	-.049	.2693	-.2569
	.0	-.054	.2691	.0217	-.055	.2691	-.2559
	4.1	.081	.2712	.0127	.100	.2647	-.2496
	8.2	.224	.2954	.0047	.263	.2605	-.2771
	12.3	.351	.3396	.0027	.416	.2569	-.3012
	16.4	.452	.3974	.0040	.546	.2534	-.2815
	20.5	.550	.4631	-.0051	.678	.2411	-.1790
High-angle adapter	20.9	.536	.4543	.0087	.663	.2333	-.3281
	20.9	.538	.4555	.0077	.665	.2336	-.3290
	31.2	.688	.6556	-.0307	.928	.2042	-.4443
	41.5	.830	.9198	-.0943	1.231	.1388	-.4850
	52.4	.807	1.1449	-.1352	1.400	.0581	-.4455
	52.5	.809	1.1485	-.1358	1.404	.0583	-.4440
	62.7	.748	1.4038	-.1901	1.590	-.0200	-.4092
	72.8	.601	1.6092	-.2463	1.715	-.0983	-.4074
	81.5	.413	1.7094	-.2820	1.752	-.1553	-.3907
	81.5	.414	1.7151	-.2809	1.758	-.1554	-.3921
	91.4	.165	1.7654	-.3195	1.761	-.2094	-.3920
	101.4	-.089	1.7968	-.3575	1.779	-.2681	-.4176
				M = 1.20			
Low-angle sting	-3.1	-0.212	0.3359	0.0493	-0.230	0.3239	-0.3849
	.0	-.077	.3137	.0316	-.077	.3137	-.3585
	.0	-.081	.3145	.0316	-.081	.3145	-.3582
	4.1	.089	.3151	.0131	.111	.3079	-.3486
	8.2	.232	.3408	.0011	.279	.3041	-.3571
	12.3	.372	.3818	-.0077	.445	.2936	-.3637
	16.5	.520	.4501	-.0234	.626	.2843	-.3106
	20.5	.589	.5073	-.0167	.729	.2685	-.2014
High-angle adapter	20.8	.576	.4975	-.0152	.715	.2601	-.3385
	20.9	.585	.5011	-.0137	.725	.2601	-.3396
	31.1	.728	.6954	-.0395	.983	.2190	-.4694
	41.3	.794	.9033	-.0816	1.192	.1545	-.4482
	52.5	.775	1.1186	-.1267	1.359	.0676	-.3765
	52.5	.776	1.1156	-.1267	1.357	.0651	-.3762
	62.7	.723	1.3637	-.1897	1.543	-.0166	-.3144
	72.8	.587	1.5726	-.2396	1.676	-.0951	-.3119
	81.5	.403	1.6653	-.2759	1.707	-.1518	-.2977
	91.4	.161	1.7199	-.3132	1.715	-.2045	-.3023
	101.4	-.086	1.7508	-.3528	1.733	-.2619	-.3399

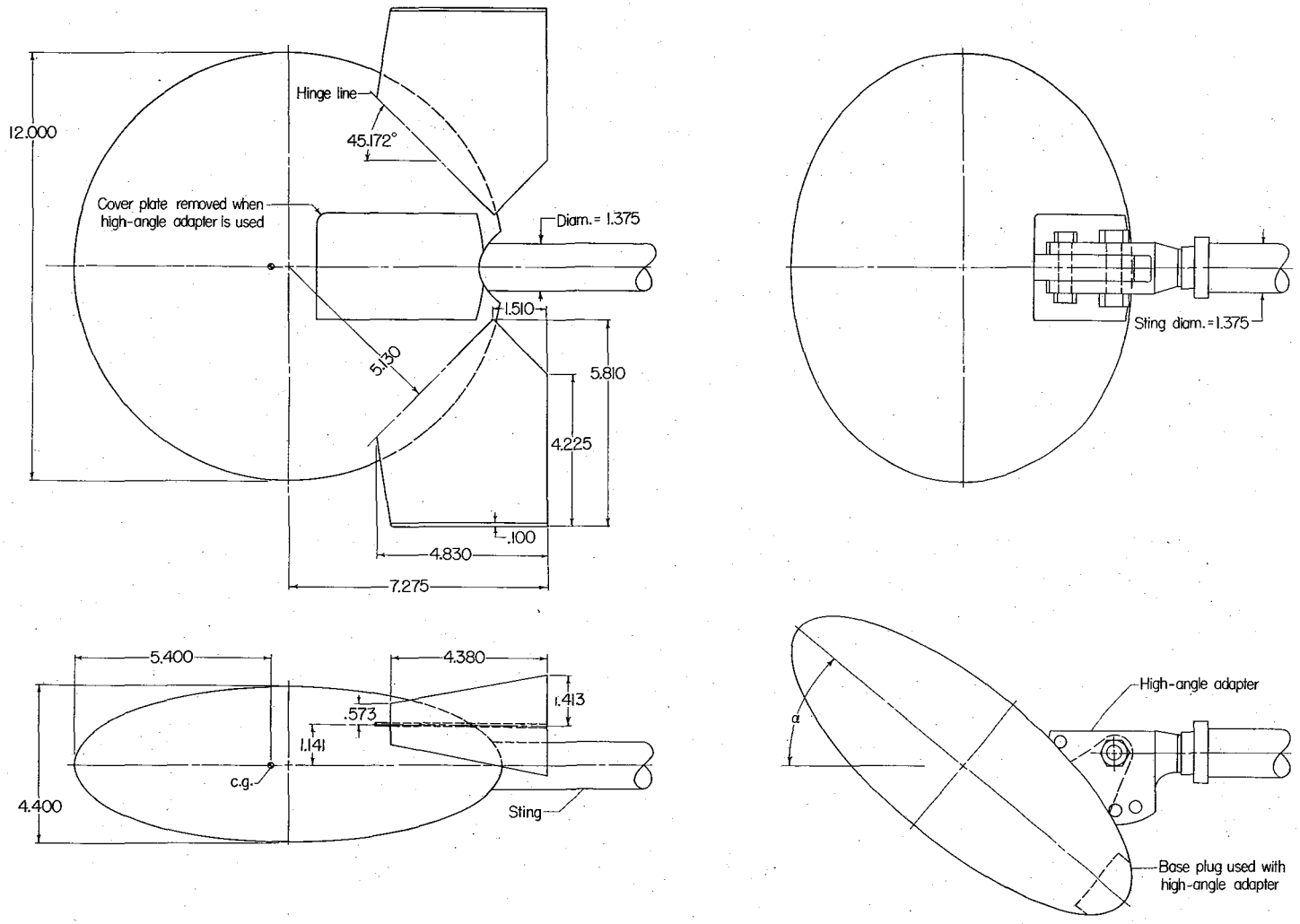
CONFIDENTIAL

TABLE III.- AERODYNAMIC COEFFICIENTS FOR THE BODY-FIN CONFIGURATION

[$\delta = -20^\circ$]

	α, deg	C_L	C_D	C_m	C_N	C_A	$C_{p,b}$
	M = 0.40						
Low-angle sting	-3.6	-0.502	0.1652	0.1008	-0.512	0.1332	0.1437
	-.1	-.425	.1305	.1205	-.425	.1297	.1937
	3.9	-.310	.0962	.1360	-.302	.1173	.2299
	8.0	-.190	.0608	.1470	-.179	.0866	.2551
	12.1	-.021	.0428	.1426	-.012	.0462	.2873
	16.1	.178	.0470	.1298	.184	-.0042	.2552
	20.2	.364	.0785	.1143	.369	-.0522	.1834
	M = 0.60						
Low-angle sting	-3.8	-0.492	0.1698	0.0994	-0.502	0.1372	0.1113
	-.2	-.414	.1354	.1204	-.414	.1339	.1717
	3.9	-.300	.1007	.1406	-.293	.1209	.2116
	8.0	-.188	.0679	.1570	-.176	.0934	.2459
	12.2	.004	.0436	.1475	.013	.0418	.2497
	16.3	.148	.0476	.1487	.155	.0044	.2369
	20.4	.350	.0839	.1332	.357	-.0435	.1731
High-angle adapter	20.6	.328	.0988	.1219	.342	-.0229	.1138
	20.6	.330	.1002	.1212	.345	-.0224	.1162
	31.1	.741	.2539	.0948	.766	-.1650	.0654
	41.1	.735	.5375	.0226	.907	-.0788	-.4247
	51.1	.619	.6927	.0332	.928	-.0460	-.4738
	51.1	.626	.6951	.0331	.934	-.0502	-.4726
	61.1	.563	.8808	.0872	1.043	-.0680	-.4920
	71.2	.502	1.0793	.1416	1.183	-.1278	-.4920
	M = 0.80						
Low-angle sting	-3.7	-0.507	0.1781	0.1054	-0.518	0.1451	0.0956
	-.1	-.394	.1425	.1242	-.394	.1415	.0808
	4.0	-.235	.1101	.1381	-.227	.1261	.0661
	8.1	-.049	.0981	.1439	-.035	.1040	.0319
	12.2	.166	.1199	.1294	.187	.0822	.0025
	16.3	.363	.1821	.0858	.400	.0728	-.1426
	20.3	.314	.2526	.0884	.382	.1282	-.2970
High-angle adapter	21.0	.362	.2050	.1114	.411	.0617	-.1262
	21.0	.365	.2076	.1112	.415	.0629	-.1335
	31.3	.468	.3904	.0846	.602	.0909	-.3939
	41.4	.461	.5505	.0356	.709	.1089	-.4371
	51.6	.524	.7614	.0203	.922	.0619	-.4935
	51.6	.525	.7634	.0204	.924	.0624	-.4943
	61.8	.530	.9753	.0818	1.110	-.0069	-.4821
	72.0	.475	1.1801	.1414	1.269	-.0862	-.4715
	M = 0.90						
Low-angle sting	-3.7	-0.414	0.2601	0.1100	-0.430	0.2332	-0.1806
	-.1	-.252	.2186	.0985	-.252	.2182	-.2021
	4.0	-.055	.1946	.0841	-.041	.1980	-.2387
	8.2	.148	.1925	.0560	.174	.1695	-.2817
	12.2	.218	.2149	.0578	.258	.1639	-.2471
	16.3	.282	.2536	.0576	.342	.1644	-.2684
	20.3	.279	.2943	.0583	.363	.1794	-.2891
High-angle adapter	21.0	.391	.3065	.0745	.475	.1463	-.4077
	21.0	.393	.3073	.0743	.477	.1465	-.4096
	31.2	.464	.4688	.0637	.640	.1603	-.4425
	41.4	.468	.6264	.0350	.765	.1609	-.4633
	51.9	.511	.8103	.0227	.953	.0976	-.4797
	51.9	.509	.8074	.0222	.949	.0976	-.4789
	62.2	.549	1.0564	.0870	1.190	.0067	-.4875
	72.4	.488	1.2730	.1520	1.361	-.0802	-.4908
	M = 0.95						
Low-angle sting	-3.7	-0.389	0.3017	0.1093	-0.408	0.2763	-0.2796
	-.1	-.188	.2570	.0816	-.188	.2568	-.2827
	4.1	.006	.2405	.0630	.023	.2395	-.3528
	8.2	.196	.2417	.0405	.228	.2114	-.3607
	12.3	.244	.2562	.0495	.293	.1985	-.3207
	16.3	.317	.2981	.0511	.388	.1971	-.3360
	20.4	.327	.3384	.0544	.424	.2035	-.3231
High-angle adapter	20.9	.422	.3707	.0645	.527	.1960	-.4656
	20.9	.420	.3676	.0638	.524	.1937	-.4633
	31.1	.456	.5190	.0652	.658	.2094	-.4638
	41.2	.447	.6555	.0244	.768	.1998	-.4585
	52.2	.556	.8863	.0349	1.041	.1046	-.5085
	52.2	.558	.8914	.0343	1.046	.1057	-.5112
	62.5	.583	1.1346	.0989	1.276	.0062	-.5124
	72.7	.512	1.3487	.1637	1.440	-.0877	-.5073

	α, deg	C_L	C_D	C_m	C_N	C_A	$C_{p,b}$
	M = 1.00						
Low-angle sting	-3.7	-0.492	0.3882	0.1539	-0.516	0.3555	-0.3162
	-.1	-.305	.3450	.1350	-.306	.3444	-.3678
	4.1	-.092	.3173	.1094	-.070	.3230	-.4114
	8.2	.143	.3065	.0660	.186	.2829	-.4506
	12.3	.275	.3164	.0505	.336	.2507	-.4094
	16.4	.374	.3638	.0504	.461	.2435	-.4160
	20.5	.454	.4222	.0496	.573	.2366	-.4399
High-angle adapter	20.8	.493	.4482	.0590	.620	.2439	-.4787
	20.8	.500	.4513	.0578	.627	.2442	-.4821
	30.9	.471	.5642	.0472	.694	.2427	-.5268
	41.1	.549	.7399	.0023	.900	.1972	-.5187
	52.3	.644	1.0052	.0486	1.189	.1053	-.5837
	52.3	.643	1.0039	.0479	1.187	.1054	-.5839
	62.5	.632	1.2177	.1131	1.372	.0019	-.5514
	72.6	.544	1.4228	.1770	1.520	-.0942	-.5317
	M = 1.03						
Low-angle sting	-3.7	-0.506	0.4020	0.1613	-0.531	0.3684	-0.3234
	-3.7	-.506	.4016	.1608	-.531	.3682	-.3230
	-3.7	-.505	.4027	.1614	-.530	.3694	-.3225
	-.1	-.334	.3630	.1458	-.335	.3624	-.3733
	-.1	-.340	.3660	.1489	-.340	.3654	-.3718
	4.0	-.121	.3326	.1179	-.097	.3402	-.4173
	8.2	.134	.3180	.0686	.178	.2957	-.4296
	12.3	.276	.3275	.0477	.340	.2612	-.4272
	16.4	.380	.2767	.0472	.471	.2542	-.4314
	20.5	.481	.4447	.0443	.606	.2485	-.4743
High-angle adapter	20.8	.498	.4547	.0554	.628	.2476	-.4493
	20.9	.503	.4575	.0545	.633	.2484	-.4501
	31.0	.536	.6048	.0360	.771	.2428	-.5607
	41.2	.638	.8063	.0136	1.011	.1863	-.5730
	52.1	.665	1.0233	.0540	1.216	.1030	-.5806
	52.1	.666	1.0239	.0537	1.217	.1030	-.5825
	62.3	.651	1.2438	.1180	1.404	.0011	-.5511
	72.5	.558	1.4539	.1825	1.555	-.0942	-.5314
	M = 1.13						
Low-angle sting	-3.7	-0.456	0.3754	0.1462	-0.479	0.3454	-0.1986
	-.1	-.294	.3369	.1312	-.295	.3364	-.2498
	4.0	-.108	.3108	.1074	-.086	.3177	-.2795
	8.2	.116	.2998	.0657	.157	.2802	-.2971
	12.3	.254	.3112	.0459	.315	.2500	-.3006
	16.4	.361	.3627	.0433	.448	.2463	-.3088
	20.5	.474	.4355	.0376	.596	.2422	-.3696
High-angle adapter	20.8	.468	.4318	.0490	.591	.2377	-.3309
	20.8	.472	.4338	.0479	.595	.2384	-.3326
	31.0	.561	.5913	.0237	.785	.2187	-.4416
	41.2	.668	.8077	.0245	1.034	.1685	-.4738
	52.2	.665	1.0106	.0599	1.206	.0932	-.4535
	52.3	.665	1.0116	.0587	1.207	.0937	-.4538
	62.5	.641	1.2246	.1194	1.382	-.0021	-.4288
	72.6	.553	1.4379	.1833	1.537	-.0972	-.4223
	M = 1.20						
Low-angle sting	-3.7	-0.481	0.4232	0.1568	-0.507	0.3914	-0.3228
	-.1	-.333	.3866	.1420	-.334	.3859	-.3401
	4.0	-.133	.3586	.1108	-.107	.3670	-.3632
	8.2	.060	.3516	.0831	.110	.3394	-.3920
	12.3	.248	.3748	.0557	.322	.3134	-.4131
	16.4	.389	.4122	.0372	.489	.2856	-.4067
	20.5	.520	.4866	.0244	.658	.2734	-.4394
High-angle adapter	20.7	.489	.4692	.0324	.623	.2658	-.3420
	20.7	.494	.4715	.0326	.629	.2658	-.3429
	31.0	.656	.6636	.0097	.904	.2309	-.4961
	41.1	.637	.7894	.0153	.999	.1766	-.4243
	52.3	.636	.9855	.0536	1.168	.1003	-.3892
	52.3	.634	.9841	.0515	1.166	.1016	-.3890
	62.5	.605	1.1773	.1081	1.324	.0082	-.3405
	72.6	.535	1.4005	.1763	1.496	-.0918	-.3368



(a) Body-fin model on low-angle sting.

(b) Body-alone model on high-angle adapter.

Figure 1.- Model details showing design dimensions. All dimensions are in inches unless otherwise noted.

CONFIDENTIAL

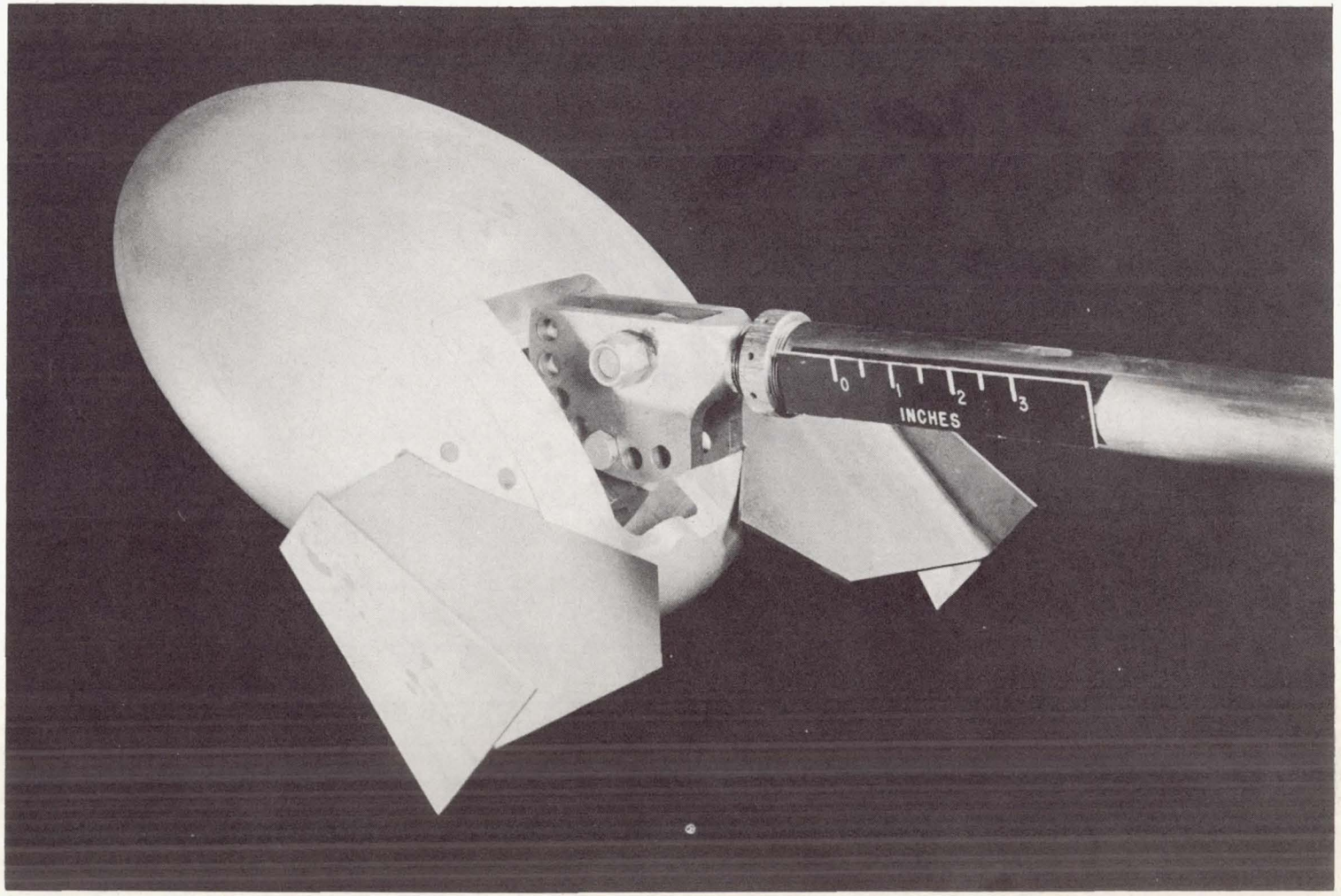
CONFIDENTIAL

(a) Body-fin model on low-angle sting L-60-1632

Figure 2.- Photographs of models.

CONFIDENTIAL

NASA-Langley, 1960 CONFIDENTIAL



(b) Body-fin model on high-angle adapter. L-60-3172

Figure 2.- Concluded.

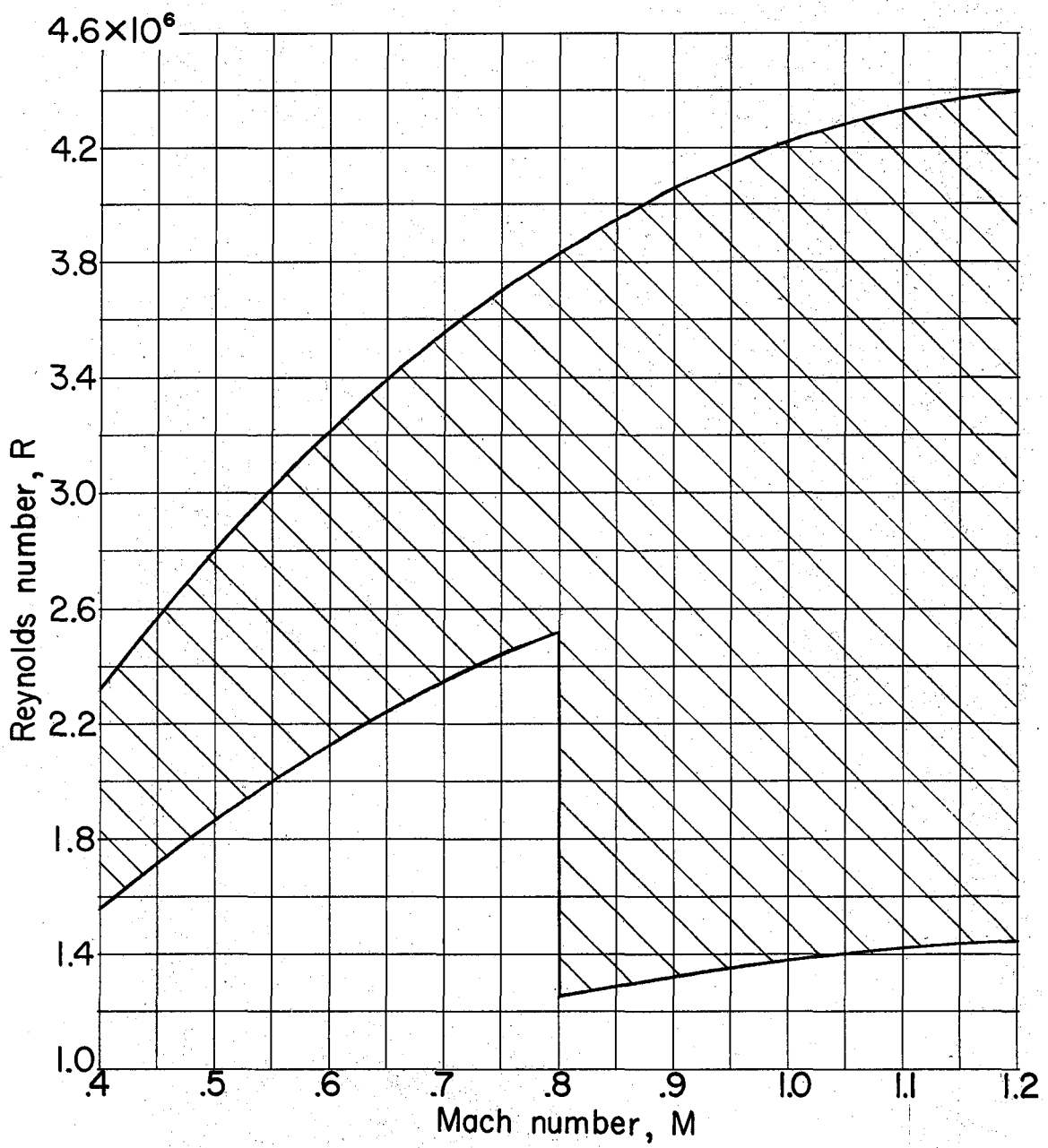


Figure 3.- Variation of Reynolds number range with Mach number. Reynolds number based on body length.

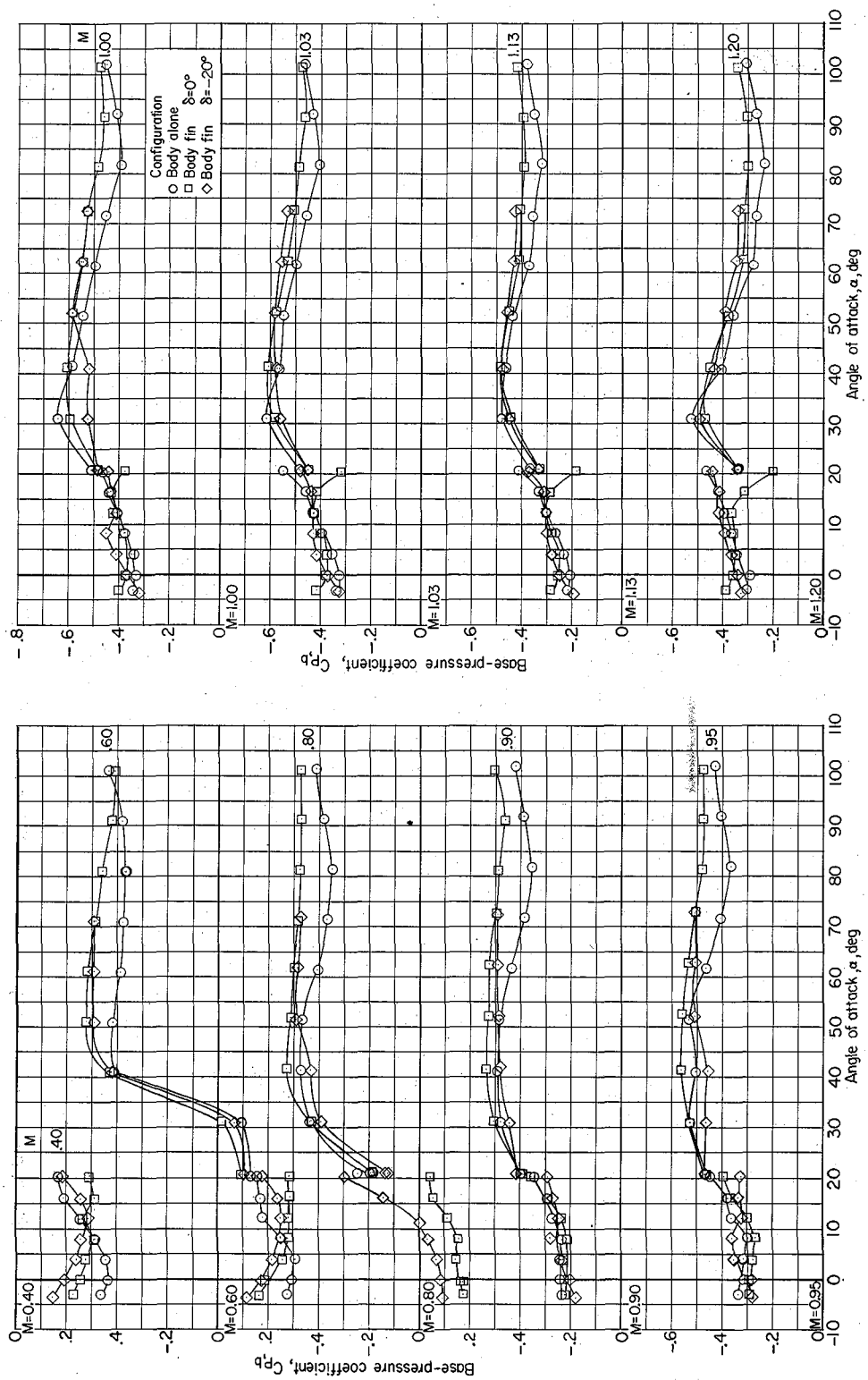
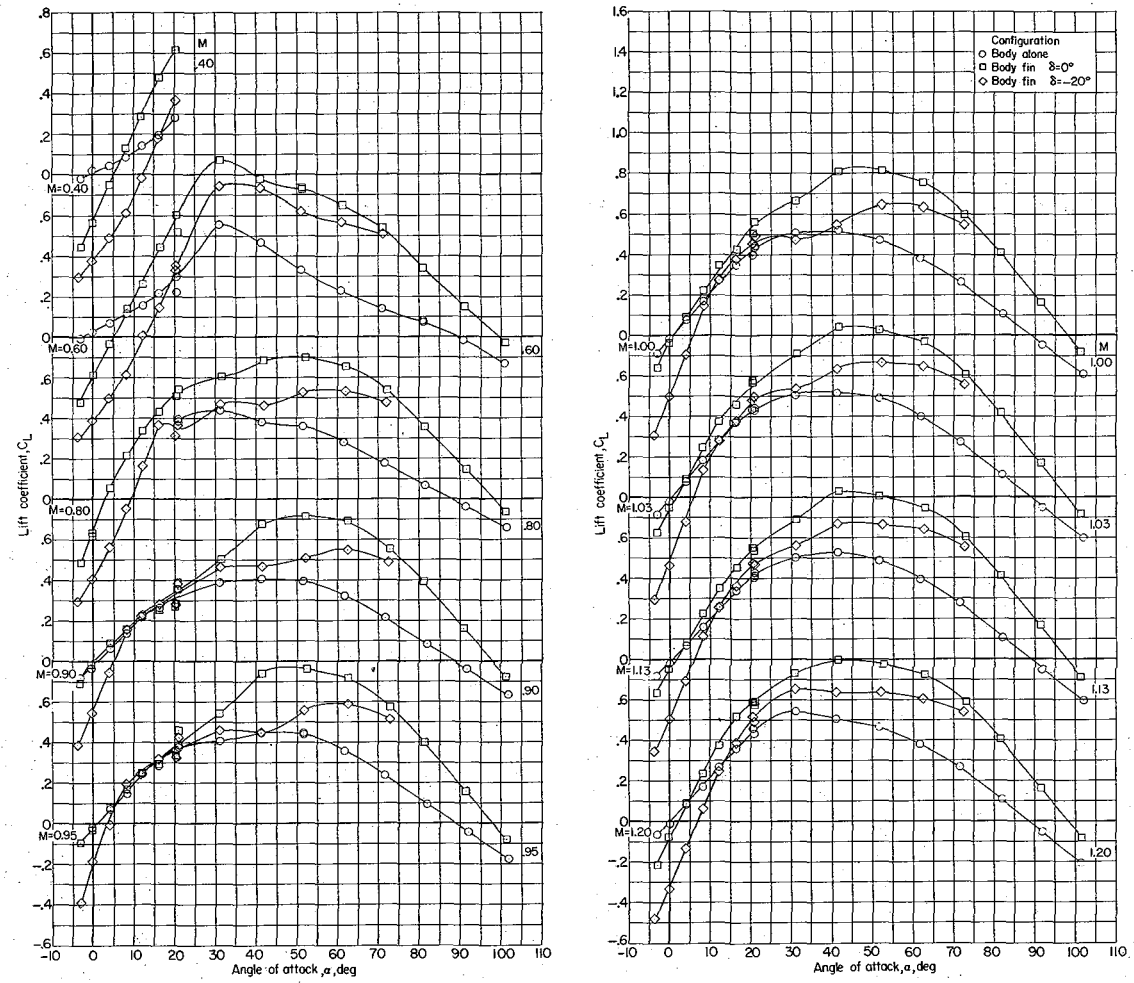


Figure 4.- Base-pressure characteristics of body-alone and body-fin configurations.

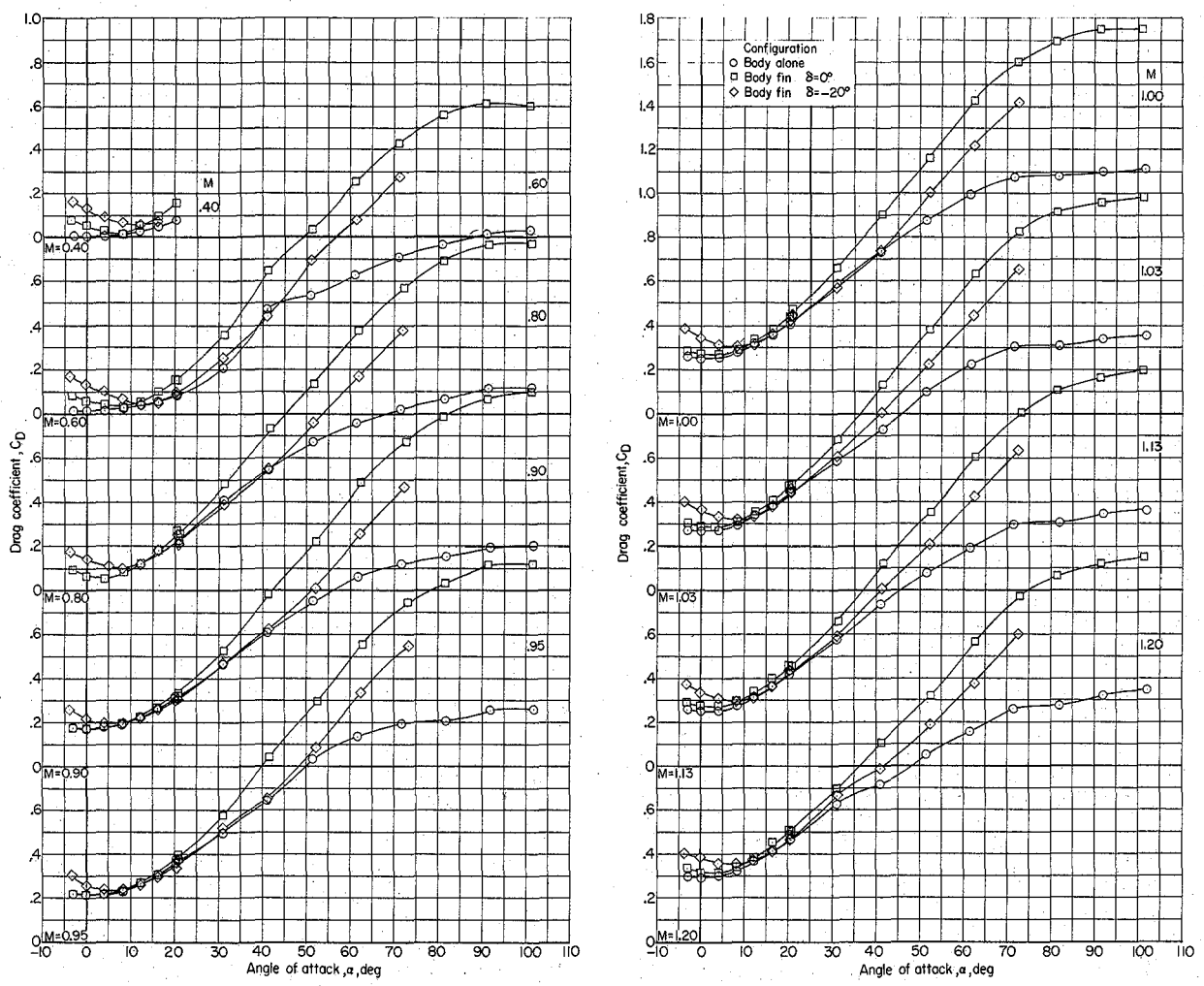
CONFIDENTIAL



(a) Lift characteristics.

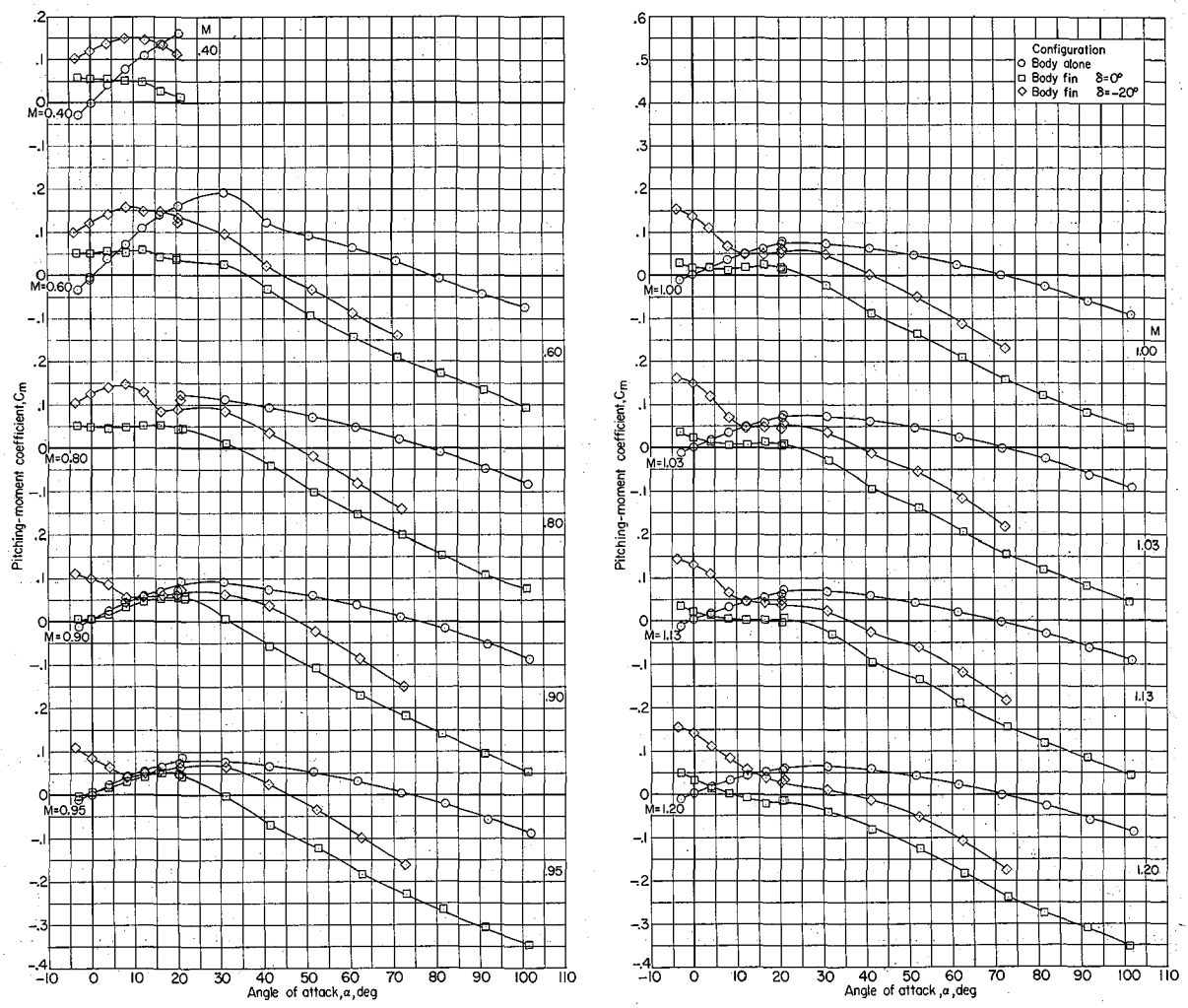
Figure 5.- Aerodynamic characteristics of body-alone and body-fin configurations.

CONFIDENTIAL



(b) Drag characteristics.

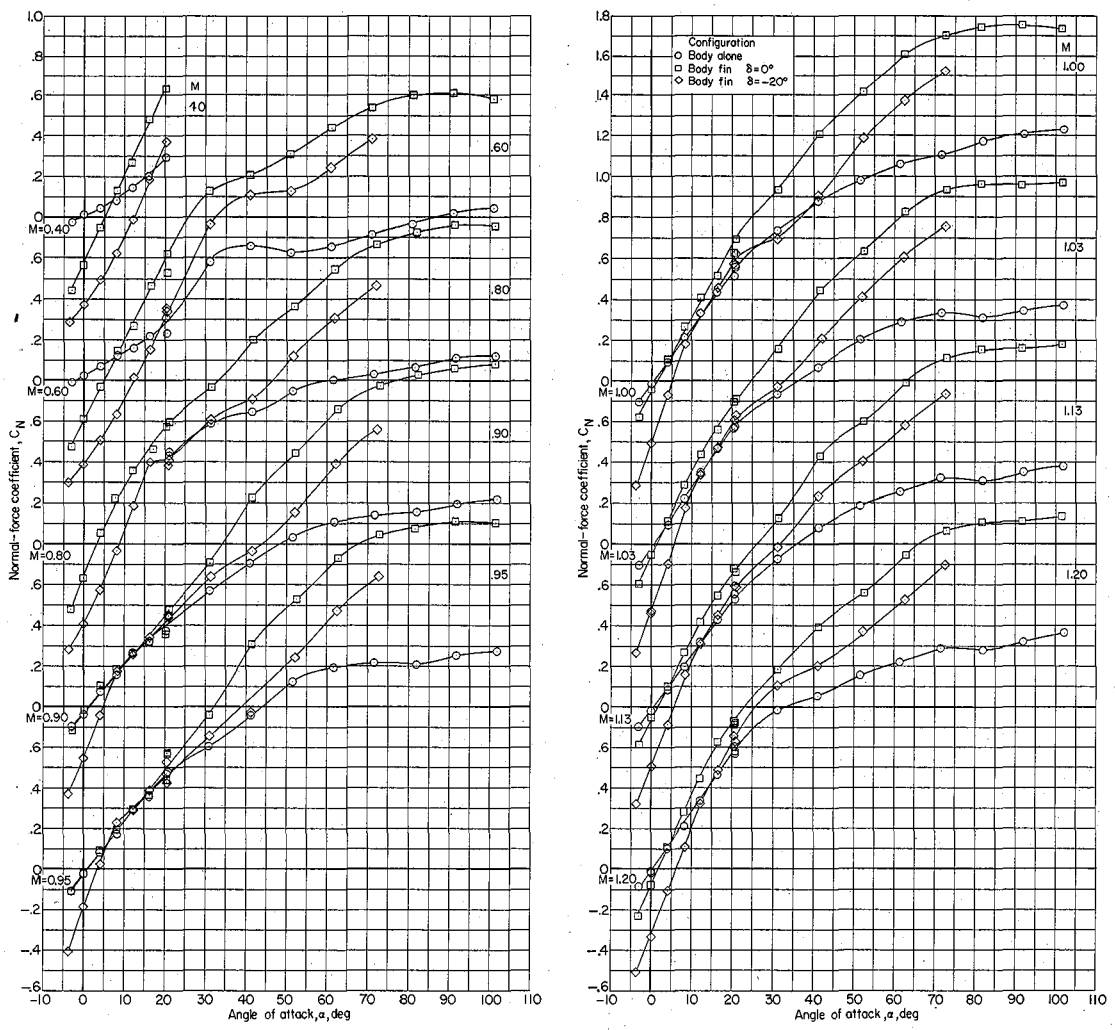
Figure 5.- Continued.



(c) Pitching-moment characteristics.

Figure 5.- Continued.

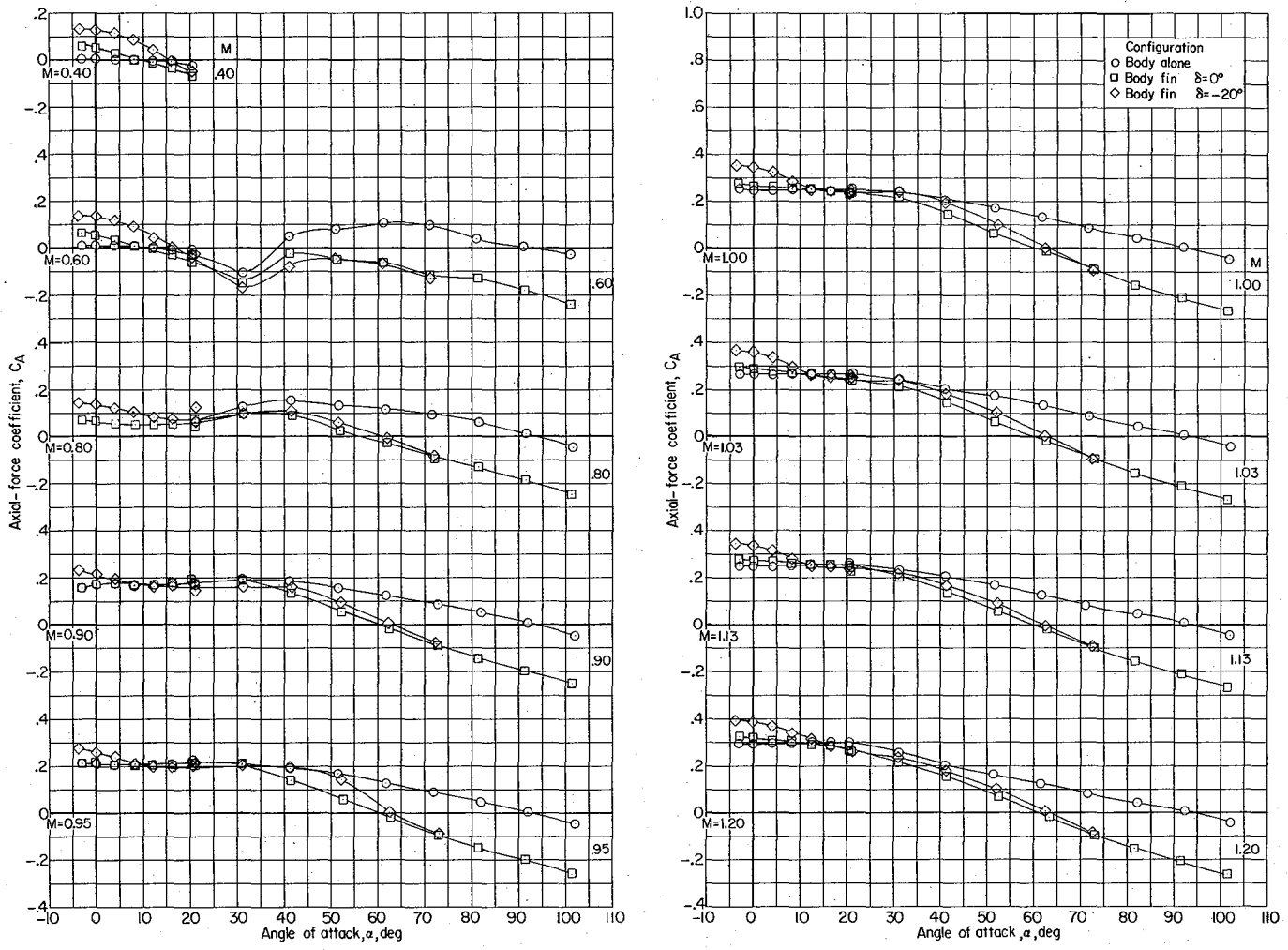
UNCLASSIFIED



(d) Normal-force characteristics.

Figure 5.- Continued.

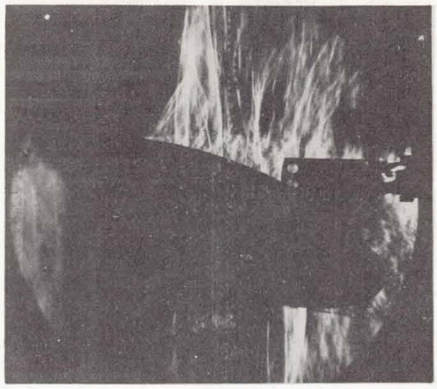
CONFIDENTIAL



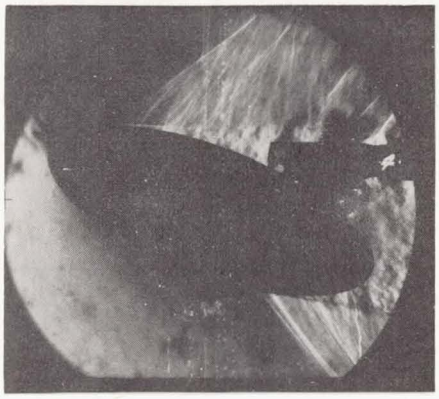
(e) Axial-force characteristics.

Figure 5.- Concluded.

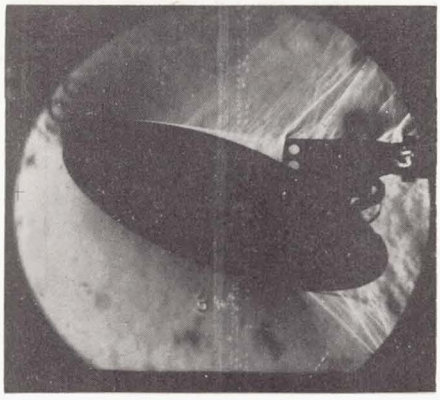
CONFIDENTIAL



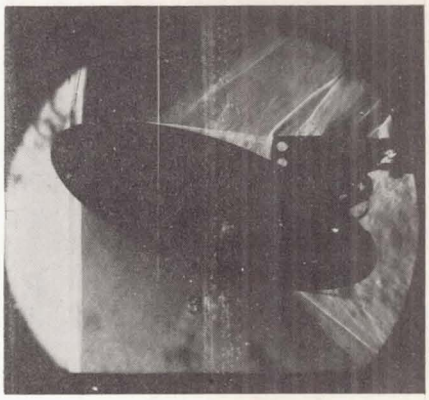
M=0.80



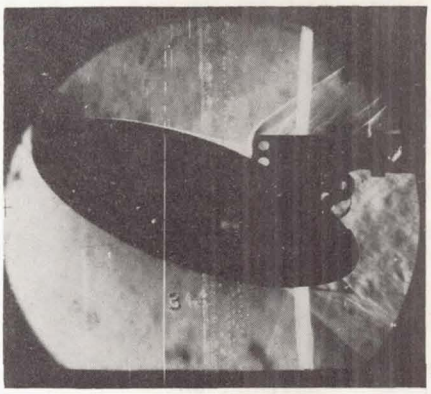
M=0.95



M=1.00



M=1.13



M=1.20

L-60-5547

Figure 6.- Schlieren photographs of the body-alone configuration. $\alpha \approx 20^{\circ}$.

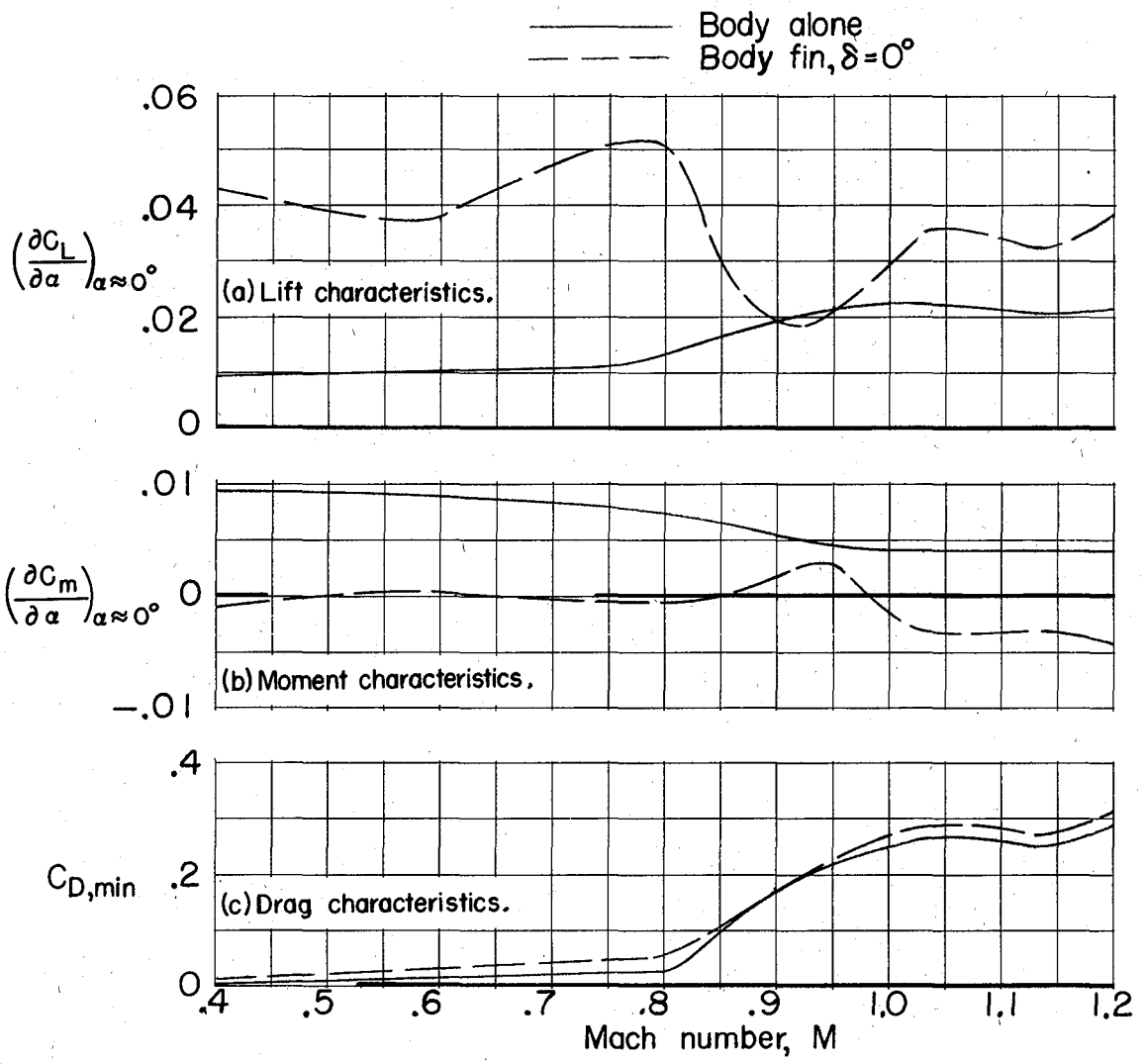


Figure 7.- Summary of the longitudinal aerodynamic parameters at low angles of attack for the body-alone and body-fin, $\delta = 0°$ configurations.

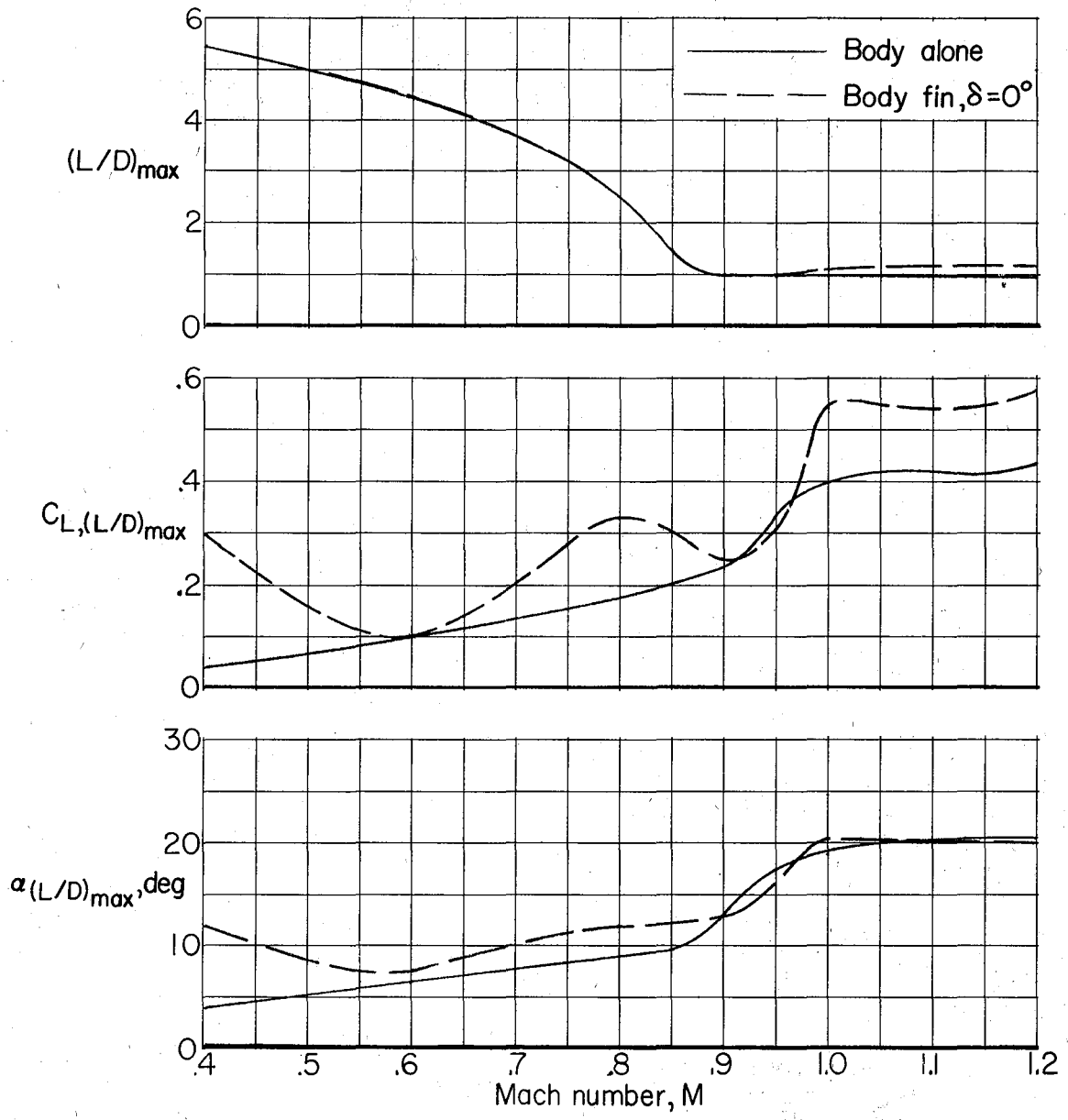


Figure 8.- Summary of maximum lift-drag-ratio characteristics for the body-alone and body-fin, $\delta = 0^{\circ}$ configurations.

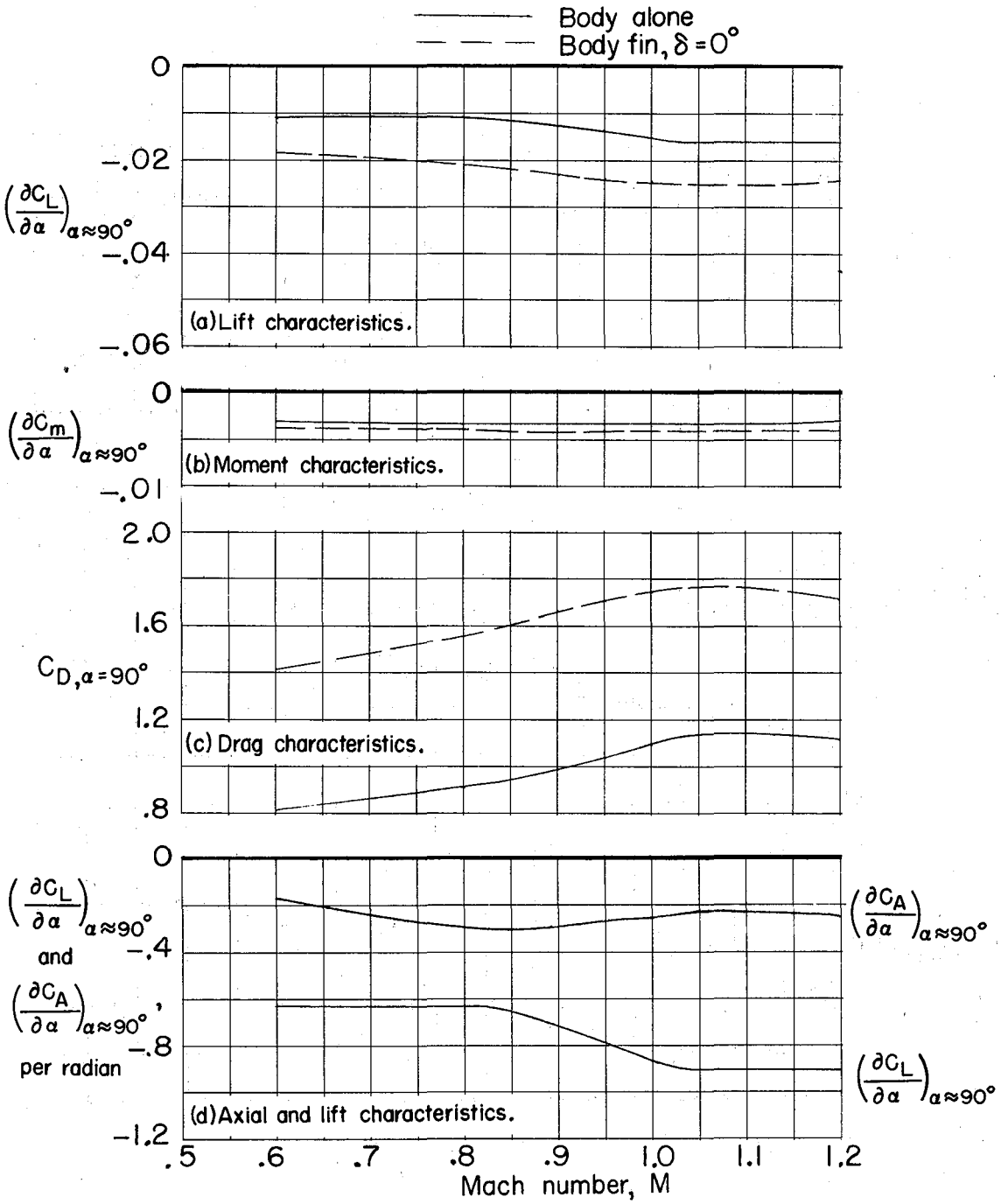


Figure 9.- Summary of the longitudinal aerodynamic parameters at an angle of attack of 90° for the body-alone and body-fin, $\delta = 0°$ configurations.

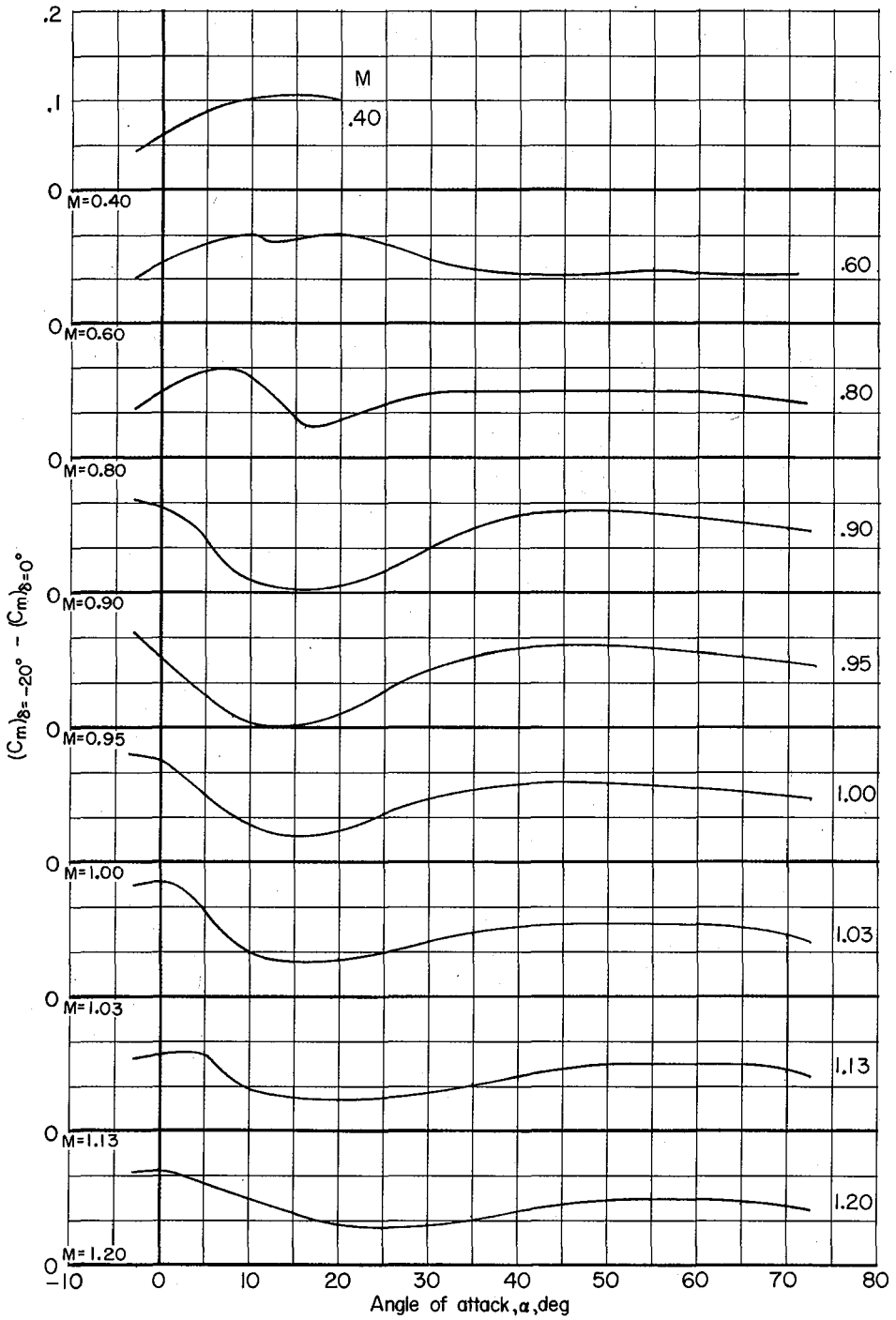


Figure 10.- Effects of a fin deflection of -20° on the pitching-moment characteristics.

UNCLASSIFIED

CONFIDENTIAL

CONFIDENTIAL